

A Geometric Analysis of Neural Collapse with Unconstrained Features

Zihui Zhu^{*,#}, Tianyu Ding^{*,◇}, Jinxin Zhou^{#,†}, Xiao Li^{†,‡}, Chong You[♣],
Jeremias Sulam[♣], and Qing Qu[†]

[#]Department of Electrical & Computer Engineering, University of Denver

[◇]Department of Applied Mathematics & Statistics, Johns Hopkins University

[‡]Center for Data Science, New York University

[♣]Google Research, New York City

[♠]Department of Biomedical Engineering & MINDS, Johns Hopkins University

[†]Department of Electrical Engineering & Computer Science, University of Michigan

May 7, 2021

Abstract

We provide the first global optimization landscape analysis of *Neural Collapse* – an intriguing empirical phenomenon that arises in the last-layer classifiers and features of neural networks during the terminal phase of training. As recently reported in [1], this phenomenon implies that (i) the class means and the last-layer classifiers all collapse to the vertices of a Simplex Equiangular Tight Frame (ETF) up to scaling, and (ii) cross-example within-class variability of last-layer activations collapses to zero. We study the problem based on a simplified *unconstrained feature model*, which isolates the topmost layers from the classifier of the neural network. In this context, we show that the classical cross-entropy loss with weight decay has a benign global landscape, in the sense that the only global minimizers are the Simplex ETFs while all other critical points are strict saddles whose Hessian exhibit negative curvature directions. In contrast to existing landscape analysis for deep neural networks which is often disconnected from practice, our analysis of the simplified model not only does it explain what kind of features are learned in the last layer, but it also shows why they can be efficiently optimized in the simplified settings, matching the empirical observations in practical deep network architectures. These findings could have profound implications for optimization, generalization, and robustness of broad interests. For example, our experiments demonstrate that one may set the feature dimension equal to the number of classes and fix the last-layer classifier to be a Simplex ETF for network training, which reduces memory cost by over 20% on ResNet18 without sacrificing the generalization performance.

*The first two authors contributed to this work equally.

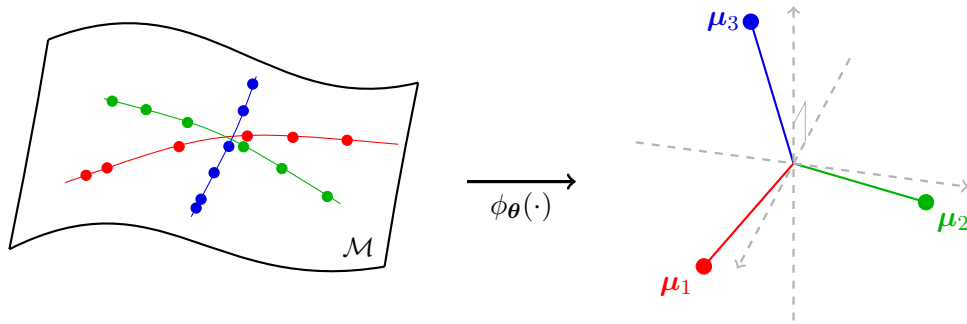


Figure 1: Illustration of Neural Collapse. Here $\phi_{\theta}(\cdot)$ denotes the feature mapping of the network, i.e. the output of the penultimate layer; see (1) for the formal definition.

1 Introduction

In the past decade, the revival of deep neural networks has led to dramatic success in numerous applications ranging from computer vision, to natural language processing, to scientific discovery and beyond [2–5]. Nevertheless, the practice of deep networks has been shrouded with mystery as our theoretical understanding for the success of deep learning remains elusive. There are many intriguing phenomena, such as implicit algorithmic bias in training [6–10], and good generalization of highly-overparameterized networks [7, 11–15], that seem often contradictory to or cannot be explained by classical optimization and learning theory.

An Intriguing Phenomenon in Deep Network Training: Neural Collapse. Towards demystifying deep neural networks (DNN), recent seminal work [1, 16] empirically discovered an intriguing phenomenon that persists across a range of canonical classification problems during the terminal phase of training. As illustrated in Figure 1, it has been widely observed that last-layer features and classifiers of a trained DNN exhibit simple but elegant mathematical structures:

- (i) **Variability Collapse:** cross-example within-class variability of last-layer features collapses to zero, as the individual features of each class themselves concentrate to their isolated class-means.
- (ii) **Convergence to Simplex ETF:** the class-means centered at their global mean are not only linearly separable, but are actually maximally distant and located on a sphere centered at the origin up to scaling (i.e., they form a Simplex Equiangular Tight Frame – or Simplex ETF).
- (iii) **Convergence to Self-duality:** the last-layer linear classifiers, living in the dual vector space to that of the class-means, are perfectly matched with their class-means.
- (iv) **Simple Decision Rule:** the last-layer classifier is behaviorally equivalent to a Nearest Class-Center decision rule.

These results suggest that deep networks are learning maximally separable features between classes, and a max-margin classifier in the last layer upon these learned features, touching the ceiling in terms of the performance. This phenomenon is referred to as *Neural Collapse (NC)* [1], and it persists across the range of canonical classification problems, on different neural network architectures

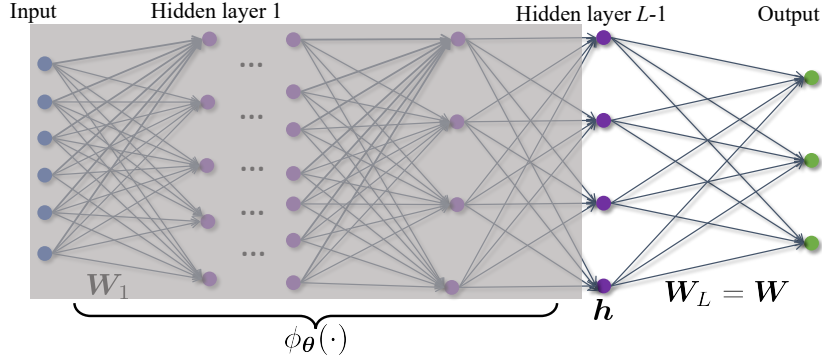


Figure 2: Illustration of the unconstrained feature model, where the gray box is peeled off so that the representation h is modeled by a simple decision variable for every training sample.

(e.g., VGG [17], ResNet [18], and DenseNet [19]) and on a variety of standard datasets (such as MNIST [20], CIFAR [21], and ImageNet [22]).

As demonstrated in [1, 23–27], the symmetric and simple mathematical structure of the last-layer classifiers could potentially lead to a profound understanding of deep networks in terms of training, generalization, and robustness. For example, it has been conjectured that the benefits of the interpolation regime of overparameterized networks might be directly related to \mathcal{NC} [1], as this behavior occurs simultaneously with the “benign overfitting” phenomenon (see [12, 28–31]); that is, when the model perfectly interpolates the training data. In addition, the variability collapse of \mathcal{NC} aligns with *information bottleneck* theory [32] which hypothesizes that neural networks seek to preserve only the minimal set of information in the learned feature representations for predicting the label hence discourage any additional variabilities. On the other hand, a recent line of work [33, 34] raises controversial questions on whether \mathcal{NC} improves robustness against data corruptions by showing that diverse features that preserve the intrinsic structure of data can better handle label corruptions. Therefore, an in-depth theoretical study of the \mathcal{NC} phenomenon could provide further insights for addressing all these fundamental questions (see Section 5 for a detailed discussion).

Towards Mathematical Analysis: Simplification via Unconstrained Feature Models. Fully demystifying the \mathcal{NC} phenomenon in theory can be very challenging. Perhaps the most difficult hurdle lies in the nonconvexity of the optimization problem for training neural networks, which, loosely speaking, stems from the nonlinear interaction across many different layers of neural networks. Towards this goal, a recent line of work [23–27] studied the properties of last-layer classifiers and features based on the assumption of the so-called *unconstrained feature model* [24] or *layer-peeled model* [27]. At a high level, the unconstrained feature model takes a *top-down* approach to the analysis of deep neural networks [23–27, 33, 34], wherein the last-layer features are modeled as *free* optimization variables (hence we call them *unconstrained features*) along with the last-layer classifiers (see Figure 2 for an illustration); this is in contrast to the conventional *bottom-up* approach that studies the problem starting from the input [35–45].¹ The underlying reasoning is that modern deep networks are often highly overparameterized with the capacity of learning any representations [46–49], so that the last-layer features can approximate, or interpolate, any point in the feature space. In this way, the model simplifies the study of last-layer features, enabling us to

¹Here, top-down means that we study the network starting from the last-layer down to the input layer, whereas bottom-up refers to an approach from the input up to the last layer.

analyze the interaction between them and the last-layer classifiers.

Nonetheless, the simplified unconstrained feature model still leaves us a highly nonconvex training loss to be dealt with. Despite the nonconvexity, recent work [24–27] studied the global minimizers, proving that Simplex ETFs (i.e., \mathcal{NC}) are indeed global solutions to the unconstrained feature model. In particular, the work [24] studied the training problem with the squared loss, proving that the gradient flow converges to \mathcal{NC} solutions with extra assumptions. Another line of work [25–27] considered the commonly used cross-entropy loss for classification, showing that the only global minimizers of the loss function are Simplex ETFs with different constraints on the weights and features.² However, these results still suffer from several limitations: (i) due to the nonconvex nature, only characterizing optimality conditions is not enough to explain the empirical global convergence of iterative algorithms to \mathcal{NC} , such as stochastic gradient descent (SGD); (ii) the problem formulations differ from those typically used by practitioners, which deploy norm regularization on the network weights (i.e., weight decay), rather than enforcing constraints, for the ease of optimization.

Contributions of This Work. Inspired by these pioneering results [1, 23–27], in this work we take a step further by characterizing the global optimization landscape of the network training loss based on the unconstrained feature model. At a high level, our contributions can be summarized as follows.

- **Benign Global Landscape.** For the unconstrained feature model, we provide the first result showing that a commonly used, regularized cross-entropy loss is a *strict saddle function* [50–52]. In other words, every critical point is either a global solution (corresponding to Simplex ETFs) or a *strict saddle point*³ with negative curvature, so that there is *no* spurious local minimizer on the optimization landscape. As summarized in Table 1, this is in contrast to previous work [24–27] that only characterizes global minimizers.
- **Efficient, Algorithmic Independent, Global Optimization.** The benign global landscape implies that any method that can escape strict saddle points (e.g. stochastic gradient descent) converges to a global solution [53] that exhibits \mathcal{NC} . This result supports our empirical observation, as shown in Section 4.1, that practical overparameterized networks always converge to ETF solutions with a diverse choice of optimization algorithms.
- **Cost Reduction for Practical Network Training.** Moreover, the universality of \mathcal{NC} implies that there is no need of training the last-layer classifiers since the weights can be simply fixed as a Simplex ETF throughout the training process. On the other hand, since \mathcal{NC} happens whenever $d \geq K$, it implies that we can choose the feature dimension d comparable to the number of classes K , reducing the feature dimension for further computational benefits. In Section 4.3, our experiments demonstrate that such a strategy achieves on par performance with classical training methods, leading to substantial cost reductions on memory and computation.

Our results shed new light on the question raised in the recent paper [54] on the role of the optimization strategy (e.g., stochastic gradient descent) for achieving \mathcal{NC} in training practical deep networks. This question also relates to the recent highly influential work [7] on the implicit algorithmic bias. For multi-class classification problems with linearly separable data, this work [7]

²The constraints on the features are mainly used to prevent it from approaching infinity since the objective function, with the cross-entropy loss, is not coercive. Note that we still refer to this model as an *unconstrained feature model* even if they include norm constraints or regularization.

³Throughout the paper, for a minimization problem, we will not distinguish between local maxima and saddle points. We call a critical point *strict saddle* if the Hessian at this critical point has at least one negative eigenvalue.

Table 1: Comparison of the setup and results under the unconstrained feature model with cross-entropy loss.

	Regularizer		Bias term	Results	
	Constraint	Weight decay		Global minimizer	Landscape
[25]	✓			✓	
[26]	✓			✓	
[27]	✓			✓	
This paper		✓	✓	✓	✓

showed that linear predictors optimized by gradient descent converge to the max-margin classifiers even without adding any explicit regularization on the cross-entropy loss. Based on this result, a sequence of works [55–62] laid great emphasis on the notion of “inductive bias” of particular optimization algorithms as a reason for the surprising success in training deep learning models.⁴ In contrast, both our theoretical result on the global landscape for the unconstrained feature model and the empirical evidence on practical deep models demonstrate that \mathcal{NC} in network training is facilitated *not only* by the choice of the optimization methods, but more importantly, by the choice of loss functions and the power of overparameterization in the network architecture.

Relationship to the Prior Arts. Our work highly relates to recent advances on studying the optimization landscape in neural network training; see [68, 69] for a contemporary survey. Most of the existing work [35–45] analyzes the problem based on a *bottom-up* approach – from the input to the output of neural networks – ranging from two-layer linear network [36, 41, 43, 70], deep linear network [37, 40, 41, 44], to nonlinear network [38, 39, 41, 42]. More specifically, the line of work [36, 37, 41, 43, 44] studied the optimization landscape for linear two-layer networks and proved that the associated training loss is a strict saddle function. For deeper linear networks, it can be shown that flat saddle points exist at the origin, but there are no spurious local minima [37, 40]. For nonlinear neural networks, it has been proved that there do exist spurious local minima [38, 39], but such local minima may be eliminated, or the number can be significantly reduced, in the overparameterization regime [38, 42]. Additionally, the work [35] proved that certain local minima (having an all-zero “slice”) are also global solutions, but the analysis is crucially dependent on the sufficient condition of an all-zero slice in the weights, which is insufficient to characterize the landscape properties. At a high level, the differences between these results and ours can be summarized as follows.

- ***A Feature Learning Perspective.*** While most of these results based on the bottom-up approach explain optimization and generalization of certain types of deep neural networks, they provided limited insights into the practice of deep learning. In contrast, we take a *top-down* approach to look at the network starting from the very last layer. The slight difference in the models can lead to a dramatic difference in the interpretability for deep learning. By starting from the last layer, our results not only provide valid reasons on why the training loss can be efficiently optimized, but also provide a precise characterization of the last-layer features as well as the classifiers learned from the network. As we will show, such a feature learning perspective not only helps with network design (see Section 4.3), but may bear broadly on generalization and robustness of deep learning as well as the recent development of contrastive learning (see Section 5).

⁴While (stochastic) gradient descent and generic steepest descent methods converge to max-margin classifiers, it should be noted that other commonly used optimization algorithms in deep learning, such as AdaGrad [63] and Adam [64], do not have max-margin properties in general and their solutions depend upon initialization, step-size and other algorithm hyper-parameters [65–67].

- **Connections to Empirical Phenomena.** Moreover, most existing theoretical results on landscape analysis [71,72] are somewhat disconnected from practice due to unrealistic assumptions, providing limited guiding principles for modern network training or design. In contrast, our assumption on the last-layer features as optimization variables is naturally based on model overparameterization. Moreover, our results provide explanations for \mathcal{NC} , an empirical phenomenon that has been widely observed on convincing numerical evidence across many different practical network architectures and a variety of standard image datasets.

Our work also broadly relates to the recent theoretical study for deep learning based on Neural Tangent Kernels (NTKs) [73], where a neural network behaves like a *linear* model on random features hence has a benign optimization landscape. However, the “kernel regime” that NTKs work in requires neural networks that are infinitely wide – or at least so wide that is beyond the regime that practical neural networks work in [74–77]. In contrast, we adopt the unconstrained feature model which does not directly impose requirements on the width of the neural network and, as shown in our experiments, well captures the behavior of practical neural networks. Hence, our result can provide a more practical understanding for deep learning.

Moreover, from a boarder perspective our work is rooted in recent advances on global non-convex optimization theory for signal processing and machine learning problems [52,78–81]. In a sequence of works [78,80,82–95], the authors showed that many problems exhibit “equivalently good” global minimizers due to symmetries and intrinsic low-dimensional structures, and the loss functions are usually strict saddles [50–52]. These problems include, but are not limited to, phase retrieval [86,87], low-rank matrix recovery [78,82,85,88,90], dictionary learning [80,83,84,91,96], and sparse blind deconvolution [92–95]. As we shall see, the global minimizers (i.e., simplex ETFs) of our problem here also exhibit a similar rotational symmetry, compared to low-rank matrix recovery. In fact, our proof techniques are inspired by recent results on low-rank matrix recovery [78,88]. Thus, our work establishes a new connection between recent advances on nonconvex optimization theory and deep learning.

Notations, Organizations, and Reproducible Research. Throughout the paper, we use bold upper and lowercase letters, such as \mathbf{X} and \mathbf{x} , to denote matrices and vectors, respectively. For a vector \mathbf{a} and a matrix \mathbf{A} , We use $\|\mathbf{a}\|_2$ and $\|\mathbf{A}\|_F$ to denote the their standard ℓ_2 -norm and Frobenius norm, respectively. Not-bold letters are reserved for scalars. The symbols \mathbf{I}_K and $\mathbf{1}_K$ respectively represent the identity matrix and the all-ones vector with an appropriate size of K , where K is some positive integer. We use $[K] := \{1, 2, \dots, K\}$ to denote the set of all indices up to K . For

any matrix $\mathbf{A} \in \mathbb{R}^{n_1 \times n_2}$, we write $\mathbf{A} = [\mathbf{a}_1 \ \dots \ \mathbf{a}_{n_2}] = \begin{bmatrix} (\mathbf{a}^1)^\top \\ \vdots \\ (\mathbf{a}^{n_1})^\top \end{bmatrix}$, so that \mathbf{a}_i ($1 \leq i \leq n_2$) and

\mathbf{a}^j ($1 \leq j \leq n_1$) denote a column vector and a row vector of \mathbf{A} , respectively. For any function $\varphi : \mathbb{R}^n \mapsto \mathbb{R}$, we use $\nabla\varphi$ and $\nabla^2\varphi$ to denote its gradient and Hessian, respectively.

The rest of the paper is organized as follows. In Section 2, we introduce the basic setup of the problem and the motivations behind our model. We present our main theoretical results in Section 3 and discuss their implications. In Section 4, we provide numerical simulations on practical neural networks to validate our theoretical findings. Finally, we conclude the paper in Section 5. We postpone all the detailed proofs to the Appendix. To reproduce the experimental results in Section 4, our code is publicly available on GitHub via the following link

<https://github.com/tding1/Neural-Collapse>.

2 The Problem Setup

In this section, we start by reviewing the basics of deep neural networks in Section 2.1, and then move onto introducing the unconstrained feature model in Section 2.2.

2.1 Basics of Deep Neural Networks

A deep neural network is essentially a *nonlinear* mapping $\psi(\cdot) : \mathbb{R}^D \mapsto \mathbb{R}^K$, which can be modeled by a composition of simple maps: $\psi(\mathbf{x}) = \psi^L \circ \dots \circ \psi^2 \circ \psi^1(\mathbf{x})$ for $\mathbf{x} \in \mathbb{R}^D$, where $\psi^\ell(\cdot)$ ($1 \leq \ell \leq L$) are called “layers”. Each layer is composed of an affine transform, represented by some weight matrix \mathbf{W}_ℓ , and bias \mathbf{b}_ℓ , followed by a simple *nonlinear*⁵ activation function $\sigma(\cdot)$. More precisely, a vanilla L -layer neural network can be written as

$$\psi_{\Theta}(\mathbf{x}) = \mathbf{W}_L \underbrace{\sigma(\mathbf{W}_{L-1} \dots \sigma(\mathbf{W}_1 \mathbf{x} + \mathbf{b}_1) + \mathbf{b}_{L-1})}_{\phi_{\theta}(\mathbf{x})} + \mathbf{b}_L. \quad (1)$$

For convenience, we use $\Theta = \{\mathbf{W}_k, \mathbf{b}_k\}_{k=1}^L$ to denote *all* the network parameters, and use $\theta = \{\mathbf{W}_k, \mathbf{b}_k\}_{k=1}^{L-1}$ to denote the network parameters up to the last layer. The output of the penultimate layer, denoted by $\phi_{\theta}(\mathbf{x})$, is usually referred to as the *representation* or *feature* of the input \mathbf{x} learned from the network. In this way, the function implemented by a neural network classifier can also be expressed as a linear classifier acting upon $\phi_{\theta}(\mathbf{x})$.

The goal of deep learning is to fit the parameters Θ so that the output of the model on an input samples \mathbf{x} approximates the corresponding output \mathbf{y} , i.e. so that $\psi_{\Theta}(\mathbf{x}) \approx \mathbf{y}$, in expectation over a distribution of input-output pairs, \mathcal{D} . This can be achieved by optimizing an appropriate loss function $\mathcal{L}(\psi_{\Theta}(\mathbf{x}), \mathbf{y})$ which quantifies this approximation. In this work, we focus on multi-class classification tasks (say, with K classes), where the class label of a sample \mathbf{x} is given by a one-hot vector $\mathbf{y} \in \mathbb{R}^K$ representing its membership to one of the K classes. In this setting, cross-entropy is one of the most popular choices for the loss function. Naturally, the distribution \mathcal{D} is unknown, but we have access to training samples that are drawn i.i.d. from \mathcal{D} . In this way, one can minimize the empirical risk over these samples by optimizing the following problem

$$\min_{\Theta} \sum_{k=1}^K \sum_{i=1}^{n_k} \mathcal{L}_{\text{CE}}(\psi_{\Theta}(\mathbf{x}_{k,i}), \mathbf{y}_k) + \frac{\lambda}{2} \|\Theta\|_F^2, \quad (2)$$

where $\mathbf{y}_k \in \mathbb{R}^K$ is a one-hot vector with only the k th entry equal to unity ($1 \leq k \leq K$), $\{n_k\}_{k=1}^K$ are the numbers of training samples in each class, and $\lambda > 0$ is the regularization parameter (or weight decay penalty), and $\mathcal{L}_{\text{CE}}(\cdot, \cdot)$ is the cross-entropy loss:

$$\mathcal{L}_{\text{CE}}(\mathbf{z}, \pi_0(\mathbf{z})) := -\log \left(\frac{\exp(z_k)}{\sum_{i=1}^K \exp(z_i)} \right), \quad (3)$$

where we assume \mathbf{z} belongs to the k th class. As introduced in Section 1, recent work [1] showed that the features learned by minimizing the above objective (i.e. $\phi_{\theta}(\mathbf{x})$) showcase the \mathcal{NC} phenomenon: their within-class variability vanishes, and the features converge to a Simplex ETF.

⁵Here, the nonlinear operator may include activations such as ReLU [97], pooling, and normalization [98], etc.

2.2 Problem Formulation Based on Unconstrained Feature Models

In deep network models, the nonlinearity and interaction between a large number of layers results in tremendous challenges for analyzing this learning problem. Since modern networks are often highly overparameterized to approximate any continuous function and the characterization of \mathcal{NC} only involves the last-layer features $\phi_{\theta}(\mathbf{x})$, a natural idea to simplify the analysis is to treat these features as free optimization variables $\mathbf{h} = \phi_{\theta}(\mathbf{x}) \in \mathbb{R}^d$, which motivates the name *unconstrained feature model*⁶ [24] (see Figure 2 for an illustration). In this way, we can rewrite the network output as $\psi_{\Theta}(\mathbf{x}) = \mathbf{W}_L \mathbf{h} + \mathbf{b}_L$.

For simplicity, we consider the setting where the number of training samples in each class is balanced (i.e., $n = n_1 = \dots = n_K$). We also write $\mathbf{W} = \mathbf{W}_L$ and $\mathbf{b} = \mathbf{b}_L$ for conciseness. Based on the unconstrained feature model, we consider a slight variant of (2), given by

$$\min_{\mathbf{W}, \mathbf{H}, \mathbf{b}} \underbrace{\frac{1}{Kn} \sum_{k=1}^K \sum_{i=1}^n \mathcal{L}_{\text{CE}}(\mathbf{W} \mathbf{h}_{k,i} + \mathbf{b}, \mathbf{y}_k)}_{:=f(\mathbf{W}, \mathbf{H}, \mathbf{b})} + \frac{\lambda_{\mathbf{W}}}{2} \|\mathbf{W}\|_F^2 + \frac{\lambda_{\mathbf{H}}}{2} \|\mathbf{H}\|_F^2 + \frac{\lambda_{\mathbf{b}}}{2} \|\mathbf{b}\|_2^2, \quad (4)$$

with $\mathbf{W} \in \mathbb{R}^{K \times d}$, $\mathbf{H} = [\mathbf{h}_{1,1} \dots \mathbf{h}_{K,n}] \in \mathbb{R}^{d \times N}$ (here, we denote $N = nK$), $\mathbf{b} \in \mathbb{R}^K$, and $\lambda_{\mathbf{W}}, \lambda_{\mathbf{H}}, \lambda_{\mathbf{b}} > 0$ are the penalty parameters for the weight decay.

As summarized in Table 1, similar optimization problems have been considered in [25–27]. In contrast to these, our problem formulation here (4), with bias and weight decay, is closer to the loss used in practice for training neural networks; existing work [25–27] considered constrained⁷ variants of (4) and without the bias term, which can be implemented but seldom used in practice due to the difficulty of optimization. In the following, we briefly discuss the differences between our simplification and practical settings for training neural networks.

- **Weight Decay on \mathbf{W} and \mathbf{H} .** One simplification of our formulation is in the weight decay. In practice, people usually impose the weight decay on all the network parameters Θ , while we enforce weight decay on the last layer’s classifier, \mathbf{W} , and features, \mathbf{H} . However, this idealization is reasonable since the energy of the features (i.e., $\|\mathbf{H}\|_F$) can indeed be upper bounded by the energy of the weights at every layer if the inputs are bounded (which holds in practice), implying that the norm of \mathbf{H} is *implicitly* penalized by penalizing the norm of Θ . Our experiments in Section 4.2 demonstrate that both approaches exhibit similar \mathcal{NC} phenomena and comparable performance in practice.
- **Treating the Last-layer Features as Optimization Variables.** One may question that “peeling off” the $L - 1$ layers might oversimplify the problem. Nonetheless, this simplification (which is also adopted in [25–27]) is based on the fact that neural networks with sufficient overparameterization can approximate any function – in Section 4.2, we numerically demonstrate that \mathcal{NC} persists even when we train overparametrized networks on randomly generated labels. Moreover, as we shall see in the following sections, both our theory and experiments demonstrate that our simplification preserves the core properties of last-layer classifiers and features during training – the \mathcal{NC} phenomenon. More specifically, in Section 3 we show that Simplex ETFs are the only global minimizers to our simplified loss function (4), and the loss function is a strict saddle function with no other spurious local minimizers so that it can be optimized efficiently to global optimality.

⁶This model is also called *layer-peeled model* in [27], where one “peels” off the first $L - 1$ layers. It has also been recently studied in [25, 26]. Throughout the paper, we will simply call it unconstrained feature model.

⁷For example, the work [27] considers inequality constraints such that the energy of \mathbf{W} and \mathbf{H} are bounded; the other work [25, 26] enforces \mathbf{W} and \mathbf{H} on the spheres up to scaling.

3 Main Theoretical Results

In this section, we present our study on global optimality conditions as well as the optimization landscape of the nonconvex loss in (4).

3.1 Global Optimality Conditions for (4)

We begin by characterizing the global solutions of (4), showing that the Simplex ETFs are its only global minimizer.

Theorem 3.1 (Global Optimality Conditions) *Assume that the feature dimension d is no smaller than the number of classes K , i.e. $d \geq K$, and the number of training samples in each class is balanced, $n = n_1 = \dots = n_K$. Then any global minimizer $(\mathbf{W}^*, \mathbf{H}^*, \mathbf{b}^*)$ of $f(\mathbf{W}, \mathbf{H}, \mathbf{b})$ in (4) satisfies*

$$\begin{aligned} w^* &:= \|\mathbf{w}^{*1}\|_2 = \|\mathbf{w}^{*2}\|_2 = \dots = \|\mathbf{w}^{*K}\|_2, \quad \text{and} \quad \mathbf{b}^* = b^* \mathbf{1}, \\ \mathbf{h}_{k,i}^* &= \sqrt{\frac{\lambda_{\mathbf{W}}}{\lambda_{\mathbf{H}} n}} \mathbf{w}^{*k}, \quad \forall k \in [K], i \in [n], \quad \text{and} \quad \bar{\mathbf{h}}_i^* := \frac{1}{K} \sum_{j=1}^K \mathbf{h}_{j,i}^* = \mathbf{0}, \quad \forall i \in [n], \end{aligned} \quad (5)$$

where either $b^* = 0$ or $\lambda_{\mathbf{b}} = 0$, and the matrix $\mathbf{W}^{*\top} \in \mathbb{R}^{d \times K}$ forms a K -Simplex ETF (defined in Definition A.1) up to some scaling and rotation, in the sense that for any $\mathbf{U} \in \mathbb{R}^{d \times d}$ with $\mathbf{U}^\top \mathbf{U} = \mathbf{I}_d$, the normalized matrix $\mathbf{M} := \frac{1}{w^*} \mathbf{U} \mathbf{W}^{*\top}$ satisfies

$$\mathbf{M}^\top \mathbf{M} = \frac{K}{K-1} \left(\mathbf{I}_K - \frac{1}{K} \mathbf{1}_K \mathbf{1}_K^\top \right). \quad (6)$$

At a high level, our proof technique finds lower bounds for the loss in (4) and studies the conditions for the lower bounds to be achieved, similar to [25, 27]. We postpone the details to Appendix B.

Remark. As can be seen in this result, any global solution of the loss function (4) exhibits \mathcal{NC} in the sense that the variability of output features $\{\mathbf{h}_{k,i}^*\}_{i=1}^n$ of each class k ($1 \leq k \leq K$) collapses to zero, and any pair of features $(\mathbf{h}_{k_1,i}^*, \mathbf{h}_{k_2,j}^*)$ from different classes $k_1 \neq k_2$ are the maximally separated, under the constraint of equal-sized angles between all classes. Similar results have been obtained in [25–27], which considered different problem formulations, as we have discussed in Section 2.2.

- **Relationship between Class Number K and Feature Dimension d .** The requirement that $d \geq K$ is necessary for Theorem 3.1 to hold, simply because K vectors in \mathbb{R}^d cannot form a K -Simplex ETF if $K > d$. However, the relationship $d \geq K$ is often true in practice. In general, and in overparameterized models in particular, the feature dimension, d , is significantly larger than the number of classes, K . For example, the dimension of the features of a ResNet [18] is typically set to $d = 512$ for CIFAR10 [21], a dataset with $K = 10$ classes. This dimension grows to $d = 2048$ for ImageNet [22], a dataset with $K = 1000$ classes.
- **Interpretations on the Bias Term \mathbf{b}^* .** In contrast to previous works [25–27], we consider the bias term in the unconstrained feature model (4). Our result indicates that a collapsing phenomenon also exists in the bias term \mathbf{b}^* , in the sense that all the elements of \mathbf{b}^* are identical. When the features \mathbf{H} are completely unconstrained, our result implies that removing the bias term \mathbf{b} has

no influence on the performance of the classifier. However, it should be noted that the ReLU unit is often applied at the end of the penultimate layer, so that \mathbf{H} should be constrained to be nonnegative, $\mathbf{H} \geq \mathbf{0}$. In such cases, $\tilde{\mathbf{h}}_i^*$ will no longer be zero, and neither will \mathbf{b}^* . Here, the bias term \mathbf{b}^* will compensate for the global mean of the features, so that the globally-centered features still form a Simplex ETF [1].⁸

3.2 Characterizations of the Benign Global Landscape for (4)

The global optimality condition in Theorem 3.1 does not necessarily mean that we can achieve these global solutions efficiently, as the problem is still nonconvex. We now investigate the global optimization landscape of (4) by characterizing all of its critical points. Our next result implies that the training loss is a strict saddle function, and every critical point is either a global minimizer or a strict saddle point that can be escaped using negative curvatures. As a consequence, this implies that the global solutions of the training problem in (4) can be efficiently found from random initializations.

Theorem 3.2 (No Spurious Local Minima and Strict Saddle Property) *Assume that the feature dimension is larger than the number of classes, $d > K$, and the number of training samples in each class is balanced $n = n_1 = \dots = n_K$. Then the function $f(\mathbf{W}, \mathbf{H}, \mathbf{b})$ in (4) is a strict saddle function with no spurious local minimum, in the sense that*

- Any local minimizer of (4) is a global minimizer of the form shown in Theorem 3.1.
- Any critical point $(\mathbf{W}, \mathbf{H}, \mathbf{b})$ of (4) that is not a local minimizer is a strict saddle with negative curvature, i.e. the Hessian $\nabla^2 f(\mathbf{W}, \mathbf{H}, \mathbf{b})$, at this critical point, is non-degenerate and has at least one negative eigenvalue, i.e. $\exists i : \lambda_i(\nabla^2 f(\mathbf{W}, \mathbf{H}, \mathbf{b})) < 0$.

In a nutshell, our proof relies on connecting the original nonconvex optimization problem to its corresponding low-rank convex counterpart, so that we can obtain the global optimality conditions for the original problem in (4) based on the convex one. With this, we can then characterize the properties of all critical points based on the optimality conditions. We defer all details of this proof to Appendix B.

Remark. Existing results [25–27] have *only* studied the global minimizers of the original problem, which has limited implication for optimization. In contrast, Theorem 3.2 characterizes the properties for *all* critical points of the function in (4). As a consequence of this result, many first-order and second-order optimization methods [99] optimizing $(\mathbf{W}, \mathbf{H}, \mathbf{b})$ are guaranteed to converge to a global solution of (4). In particular, the result in [50, 53] ensures that (stochastic) gradient descent with random initialization, the *de facto* optimization algorithm used in deep learning, almost surely escapes strict saddles and converges to a second-order critical point – which happens to be a global minimizer of form showed in Theorem 3.1 for our problem (4).

- **Constructing the Negative Curvature Direction for Strict Saddles.** One of the major difficulties in our proof is to construct the negative curvature direction for strict saddle points. Here, we exploit the fact that the feature dimension d is larger than the number of classes K , and construct

⁸Suppose that an optimal solution to (4) is $(\mathbf{W}^*, \mathbf{H}^*, \mathbf{b}^*)$, satisfying the conditions in Theorem 3.1. There exists a nonzero vector $\alpha \in \mathbb{R}^d$ such that $\tilde{\mathbf{H}}^* = \mathbf{H}^* + \alpha \mathbf{1}^\top \geq \mathbf{0}$. Here, α can be viewed as the global mean of $\tilde{\mathbf{H}}^*$ since \mathbf{H}^* has mean zero. Then, let $\tilde{\mathbf{b}}^* = -\mathbf{W}^* \alpha$, so that $\tilde{\mathbf{W}}^* \tilde{\mathbf{H}}^* + \tilde{\mathbf{b}}^* \mathbf{1}^\top = \mathbf{W}^* \mathbf{H}^* + (\mathbf{W}^* \alpha + \tilde{\mathbf{b}}^*) \mathbf{1}^\top = \mathbf{W}^* \mathbf{H}^*$. Therefore, we can see that $(\tilde{\mathbf{W}}^*, \tilde{\mathbf{H}}^*, \tilde{\mathbf{b}}^*)$ achieves the same cross-entropy loss as $(\mathbf{W}^*, \mathbf{H}^*, \mathbf{b}^*)$.

the negative curvature direction within the null space of $\mathbf{W} \in \mathbb{R}^{K \times d}$. This is also the main reason for the requirement $d > K$ in Theorem 3.2, but we conjecture the results also hold for $d = K$ and could be proved with more sophisticated analysis, which is left as future work.

- **Relationship to Low-Rank Matrix Recovery.** As discussed in Section 1, it has been recently shown that the strict saddle property holds for a wide range of nonconvex problems in machine learning [78,80,82–92,96], including low-rank matrix recovery [78,89,100–103]. As we know that $\|\mathbf{Z}\|_* = \min_{\mathbf{Z}=\mathbf{W}\mathbf{H}} \frac{1}{2} \left(\|\mathbf{W}\|_F^2 + \|\mathbf{H}\|_F^2 \right)$ (see [35] for a proof), our formulation in (4) is closely related to low-rank matrix problems [78,89,100–103] with the Burer-Moneirto factorization approach [104], by viewing \mathbf{W} and \mathbf{H} as two factors of a matrix $\mathbf{Z} = \mathbf{W}\mathbf{H}$. The differences lie in the loss functions and statistical properties of the problem.⁹ Therefore, our result establishes a connection between the study of low-rank matrix factorization and neural networks under the unconstrained feature model.
- **Comparison to Existing Landscape Analysis on Neural Network.** Section 1 provided a comprehensive discussion on the relationship between our result and previous works on landscape analysis for deep neural networks. Although the unconstrained feature model can be viewed as a two-layer linear network with input being the columns of an identity matrix, as precluded in Section 1, our result has much broader implications than the previous results [36,37,40,41,43,44,70]. First, our problem formulation (4) is closer to practical settings for classification tasks, which considers the widely adopted cross-entropy loss while including weight decay and a bias term, while most existing results [36,37,40,41,43,44,70] either do not incorporate any regularization and bias, or focus on the squared loss for the regression problem. More importantly, our result characterizes the precise form of the global solutions (i.e., \mathcal{NC}) for the last layer features and classifiers, and shows that they can be efficiently achieved. Moreover, convincing numerical results in [1] and the next section demonstrate that the global solutions do appear and can be achieved by practical networks on various standard image datasets. Our study of last-layer features could have profound implications for studying generalization and robustness of the deep networks.

4 Experiments

In this section, we run extensive experiments not only verifying our theoretical discoveries on modern neural networks, but also demonstrating the potential practical benefits of understanding \mathcal{NC} . More specifically, while Theorem 3.2 is for the simplified models, in Section 4.1 we run experiments on practical network architectures and show that our analysis of simplified models captures the core \mathcal{NC} on practical network architectures that the prevalence of \mathcal{NC} is due to the geometry rather than the algorithmic bias, by showing that different type of optimization algorithms (e.g., SGD, Adam, and limited-memory BFGS (LBFGS) [99]) *all* achieve \mathcal{NC} during the terminal phase of training. In Section 4.2, we verify the validity of the simplification based on the unconstrained feature model in Section 2.2. Moreover, the universality of \mathcal{NC} implies that there is no need for training the last-layer classifiers since the weights can be simply fixed as a Simplex ETF throughout the training process. In Section 4.3, we demonstrate that such a strategy achieves essentially

⁹We consider the cross-entropy loss rather than the least-squares loss due to the differences in the task – we focus on classification instead of recovery problems. On the other hand, the results on low-rank matrix recovery are often based on certain statistical properties, such as the randomness in the measurements [100,101], or restricted well-conditionedness property of the objective function [88,103]. In contrast, these statistical properties do not exist in our problem, where the model and analysis are purely deterministic.

the same generalization performance as classical training algorithms, while improving on memory and computation. We begin by describing the basic experimental setup, including the network architectures, evaluation datasets, training procedures, and metrics for measuring \mathcal{NC} .

Setup of Network Architectures, Dataset, and Training. In Section 4.1 and Section 4.2, we train the cross-entropy loss (2) on ResNet18 architecture [18] on MNIST [105] and CIFAR10 [21] datasets for the classical image classification task. Without explicitly mentioning, the images are normalized (channel-wise) by their mean and standard deviation. We include no data augmentation in this section, because our focus is to study the behavior associated with \mathcal{NC} instead of obtaining state-of-the-art performance. In Section 4.3, We train the cross-entropy loss (2) on the same ResNet18 architecture on MNIST and a modified version¹⁰ of ResNet50 [106] architecture on CIFAR10 datasets for the classical image classification task. For fair comparisons with the results reported on CIFAR10, we use the same data augmentation in [107]. We train the network for 200 epochs with three distinct optimizers: two first-order methods (SGD and Adam) and one second-order method (LBFGS). In particular, we use SGD with momentum 0.9, Adam with $\beta_1 = 0.9, \beta_2 = 0.999$, and LBFGS with a memory size of 10. The initial learning rates for SGD and Adam are set to 0.05 and 0.001, respectively, and decreased by a factor of 10 for every 40 epochs. For LBFGS, we use an initial learning rate of 0.1 and employ a strong Wolfe line-search strategy for subsequent iterations. Except otherwise specified, the weight decay is set to 5×10^{-4} for all the experiments.

Metrics for Measuring \mathcal{NC} During Network Training. We measure \mathcal{NC} for the learned last-layer classifiers and features based on the properties presented in Section 1. Some of the metrics are similar to those presented in [1]. First, we define the global mean and class mean of the last-layer features $\{\mathbf{h}_{k,i}\}$ as

$$\mathbf{h}_G = \frac{1}{nK} \sum_{k=1}^K \sum_{i=1}^n \mathbf{h}_{k,i}, \quad \bar{\mathbf{h}}_k = \frac{1}{n} \sum_{i=1}^n \mathbf{h}_{k,i} \quad (1 \leq k \leq K).$$

- **Within-class Variability Collapse for the Learned Features \mathbf{H} .** We introduce the within-class and between-class covariance matrices as

$$\Sigma_W := \frac{1}{nK} \sum_{k=1}^K \sum_{i=1}^n (\mathbf{h}_{k,i} - \bar{\mathbf{h}}_k) (\mathbf{h}_{k,i} - \bar{\mathbf{h}}_k)^\top, \quad \Sigma_B := \frac{1}{K} \sum_{k=1}^K (\bar{\mathbf{h}}_k - \mathbf{h}_G) (\bar{\mathbf{h}}_k - \mathbf{h}_G)^\top.$$

Thus, we can measure the within-class variability collapse by measuring the magnitude of the between-class covariance $\Sigma_B \in \mathbb{R}^{d \times d}$ compared to the within-class covariance $\Sigma_W \in \mathbb{R}^{d \times d}$ of the learned features via

$$\mathcal{NC}_1 := \frac{1}{K} \text{trace} \left(\Sigma_W \Sigma_B^\dagger \right), \quad (7)$$

where Σ_B^\dagger denotes the pseudo inverse of Σ_B .

- **Convergence of the Learned Classifier \mathbf{W} to a Simplex ETF.** For the learned classifier $\mathbf{W} \in \mathbb{R}^{K \times d}$, we quantify its closeness to a Simplex ETF up to scaling by

$$\mathcal{NC}_2 := \left\| \frac{\mathbf{W}\mathbf{W}^\top}{\|\mathbf{W}\mathbf{W}^\top\|_F} - \frac{1}{\sqrt{K-1}} \left(\mathbf{I}_K - \frac{1}{K} \mathbf{1}_K \mathbf{1}_K^\top \right) \right\|_F, \quad (8)$$

¹⁰Here, we use a modified version because the original ResNet50 [18] is fine-tuned for ImageNet dataset [22] which does not achieve performance on CIFAR10.

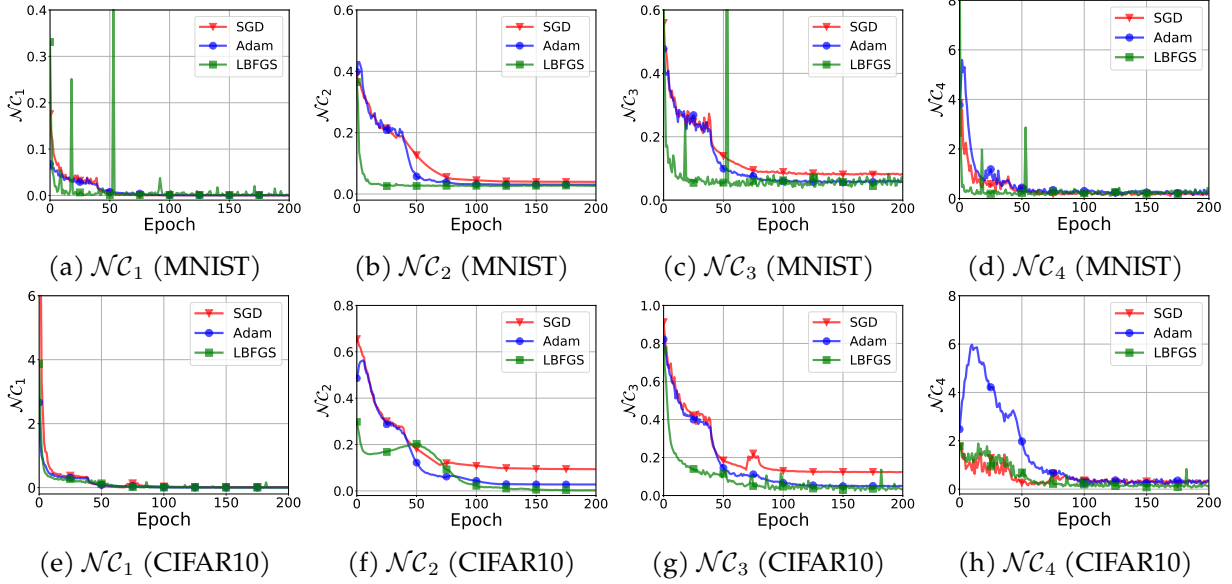


Figure 3: **Illustration of \mathcal{N} across different training algorithms** with ResNet18 on MNIST (top) and CIFAR10 (bottom). From the left to the right, the plots show the four metrics, \mathcal{N}_1 , \mathcal{N}_2 , \mathcal{N}_3 , and \mathcal{N}_4 , for measuring \mathcal{N} , defined in (7), (8), (9), and (10), respectively.

where we rescale the ETF in (6) so that $\frac{1}{\sqrt{K-1}} (\mathbf{I}_K - \frac{1}{K} \mathbf{1}_K \mathbf{1}_K^\top)$ has unit energy (in Frobenius norm). It should be noted that our metric \mathcal{N}_2 combines two metrics used in [1] to quantify to what extent the classifier approaches equiangularity and maximal-angle equiangularity.

- **Convergence to Self-duality.** Next, we measure the collapse of the learned features \mathbf{H} to its dual \mathbf{W} . Let us define the centered class-mean matrix as

$$\bar{\mathbf{H}} := [\bar{\mathbf{h}}_1 - \mathbf{h}_G \quad \cdots \quad \bar{\mathbf{h}}_K - \mathbf{h}_G] \in \mathbb{R}^{d \times K}.$$

Thus, we measure the duality between the classifiers \mathbf{W} and the centered class-means $\bar{\mathbf{H}}$ by

$$\mathcal{N}_3 := \left\| \frac{\mathbf{W}\bar{\mathbf{H}}}{\|\mathbf{W}\bar{\mathbf{H}}\|_F} - \frac{1}{\sqrt{K-1}} \left(\mathbf{I}_K - \frac{1}{K} \mathbf{1}_K \mathbf{1}_K^\top \right) \right\|_F. \quad (9)$$

- **Collapse of the Bias.** In many cases, the global mean \mathbf{h}_G of the features might not be zero,¹¹ and the bias term \mathbf{b} would compensate for the global mean \mathbf{h}_G in the sense that

$$\mathbf{W}\mathbf{h}_{k,i} + \mathbf{b} = \mathbf{W}(\mathbf{h}_{k,i} - \mathbf{h}_G) + \underbrace{\mathbf{W}\mathbf{h}_G + \mathbf{b}}_{=0}.$$

Thus, we capture this collapsing phenomenon by measuring

$$\mathcal{N}_4 := \|\mathbf{b} + \mathbf{W}\mathbf{h}_G\|_2. \quad (10)$$

¹¹For example, as discussed after Theorem 3.1 all the feature vectors in \mathbf{H} would be nonnegative, because the non-negative nonlinear operator ReLU has been applied at the end of the penultimate layer.

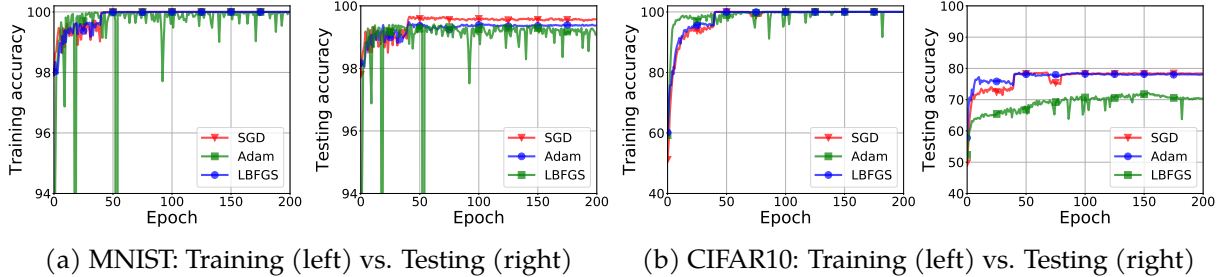


Figure 4: **Illustrations of training and test accuracy** for three different training algorithms (i.e., SGD, Adam, and LBFGS) with ResNet18 on MNIST and CIFAR10.

4.1 The Prevalence of \mathcal{NC} Across Different Optimization Algorithms

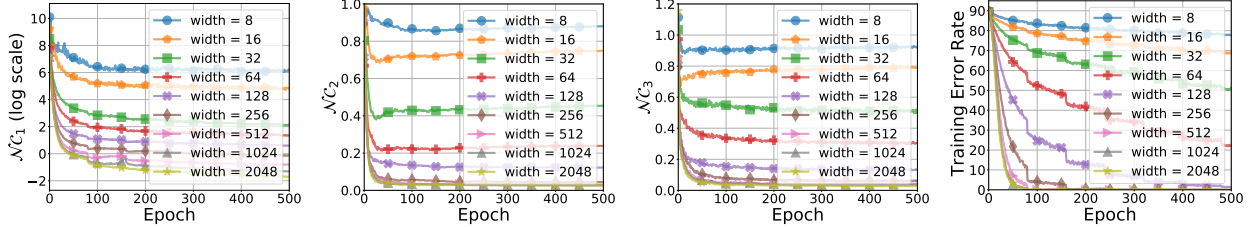
Our result in Theorem 3.2 reveals a benign global landscape for the optimization of neural networks under the unconstrained feature model, which further implies that the prevalence of \mathcal{NC} is independent of the choice of particular training methods. In this subsection, we validate our theoretical discovery on modern network architectures and standard datasets. We show different types of training methods (e.g., SGD, Adam, and LBFGS) all achieve \mathcal{NC} during the terminal phase of training. In Figure 3 and Figure 4, we run all the experiments with ResNet18 on MNIST and CIFAR10 without modification. The results lead to the following observations:

- **\mathcal{NC} is Algorithm Independent.** Figure 3 shows the evolution of the four metrics $\mathcal{NC}_1, \mathcal{NC}_2, \mathcal{NC}_3,$ and \mathcal{NC}_4 , for measuring \mathcal{NC} as training progresses, defined in (7), (8), (9), and (10), respectively. We consistently observe that all four metrics collapse to zero, trained by different types of algorithms – SGD, Adam, and LBFGS. This implies that \mathcal{NC} happens regardless of the choice of training methods. The last-layer features learned by the network are always maximally linearly separable, and correspondingly the last-layer classifier is a perfect linear classifier for the features.
- **Relationship between \mathcal{NC} and Generalization.** Figure 4 depicts the learning curves in terms of both the training and test accuracy for all three optimization algorithms (i.e., SGD, Adam, and LBFGS). These experimental results¹² show that different training algorithms learn neural networks with notably different generalization performances, even though all of them exhibit \mathcal{NC} . Since \mathcal{NC} is only a characterization of the training data, it does not directly translate to unseen data. As the network is highly overparameterized, there are infinitely many networks that produce the same \mathbf{H} with \mathcal{NC} for a particular training dataset, but with different generalization performance. This suggests that study generalization needs to consider the algorithmic bias and the learned weights for the feature \mathbf{H} . A thorough investigation between \mathcal{NC} and generalization is the subject of future work.

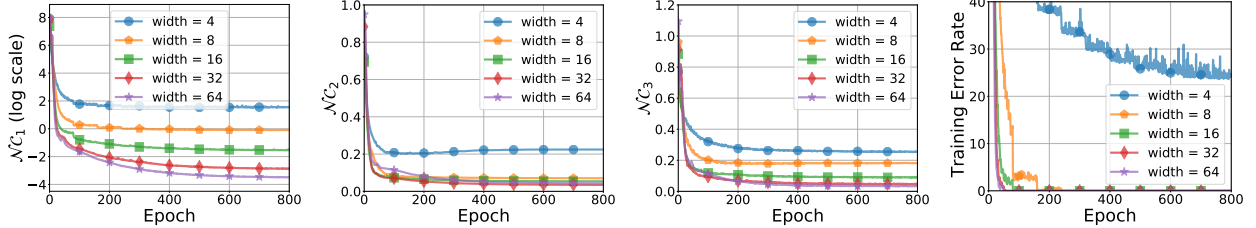
4.2 The Validity of (4) Based on Unconstrained Feature Models for \mathcal{NC}

The premise of our global landscape analysis of (4) for studying \mathcal{NC} in deep neural networks is based upon the unconstrained feature model introduced in Section 2.2, which simplifies the network by synthesizing the first $L - 1$ layers as a universal approximator that generates a simple

¹²Note that here we use the default version of LBFGS in PyTorch. Other variants of quasi-Newton methods [108,109] may give different or better generalization performance.



(a) Random Label CIFAR10-MLP (from left to right): $\mathcal{N}C_1$ (log scale), $\mathcal{N}C_2$, $\mathcal{N}C_3$, Training Error Rate



(b) Random Label CIFAR10-ResNet18 (from left to right): $\mathcal{N}C_1$ (log scale), $\mathcal{N}C_2$, $\mathcal{N}C_3$, Training Error Rate

Figure 5: **Training results of CIFAR10 with completely random label.** Multilayer perceptron (MLP) of a fixed depth of 4 (top) and ResNet18 (bottom) models are used with various feature width. Note that the right column is the misclassification percentage of all samples in training.

decision variable for each training sample. Here, we demonstrate through experiments that such a simplification is reasonable for overparameterized networks, at least sufficient for characterizing $\mathcal{N}C$ in practical network training.

The Validity of Unconstrained Feature Models. First, we demonstrate that overparameterization is crucial for $\mathcal{N}C$ phenomenon during network training, while the input plays minimal influence. These provide numerical supports on treating \mathbf{H} as a free optimization variable for studying $\mathcal{N}C$. In particular, we modify the training dataset CIFAR10 by replacing *all* the correct label for each training sample with a *random* counterpart. For the ease of studying the effects of model sizes (i.e., overparameterization) on $\mathcal{N}C$, besides ResNet18 networks¹³, we train 4-layer multilayer perceptrons (MLP) of different network width using SGD with learning rate 0.01 and weight decay 10^{-4} . We report the corresponding $\mathcal{N}C$ behaviors in Figure 5, which shows how training misclassification rate and $\mathcal{N}C$ evolve over epochs of training for networks with different widths. As the network is sufficiently large, it has enough capacity to memorize the training data and achieves zero training error, which is consistent with the observations in [11]. Moreover, we find from Figure 5 that the training accuracy is highly correlated with $\mathcal{N}C$ in the sense that a larger network (i.e., larger width) tends to exhibit severe $\mathcal{N}C$ and achieves smaller training error. In other words, while the emerging consensus is that the network can memorize any training data, our results show that such memorization happens in a particular way – the features are maximally separated, followed by a max-margin linear classifier.

Comparison of Weight Decay on the Network Parameter Θ vs. on the Features \mathbf{H} in (4). In comparison to typical training protocols of deep networks which enforce weight decay on all the network weights Θ , our problem formulation (4) based on the unconstrained feature model replaced Θ by penalizing the feature \mathbf{H} produced by the $L - 1$ “peeled-off” layers. To check the

¹³Here, for ResNet18 we adopt the method in [15] to change its network width.

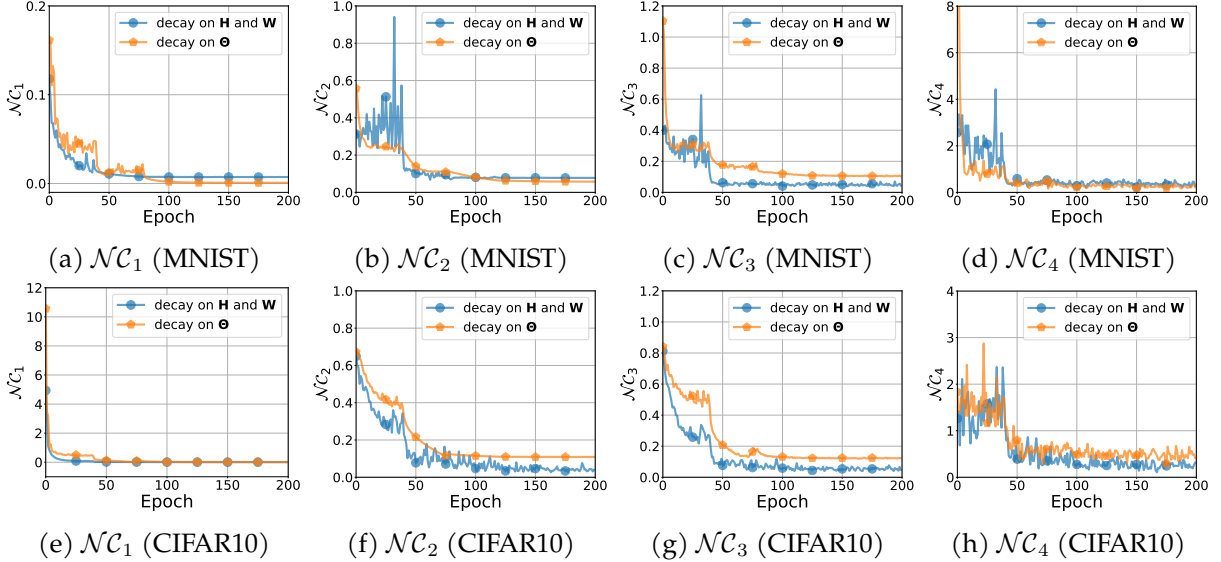


Figure 6: **Comparison of $\mathcal{N}\mathcal{C}$ behavior for weight decay on Θ vs. on (H, W) .** For the latter set up, we choose $\lambda_W = \lambda_b = 0.01$ and $\lambda_H = 0.00001$.

practicality of such formulation, we empirically run experiments using ResNet18 on MNIST and CIFAR10. Figure 6 shows the $\mathcal{N}\mathcal{C}$ evolution for both the classical formulation and our “peeled” formulation, we notice that the $\mathcal{N}\mathcal{C}$ behavior happens in both scenarios comparably. We also point that without extensive hyper-parameter tuning, the models trained under the “peeled” set-up could already achieve test accuracy of 99.57% and 77.92% on MNIST and CIFAR10 respectively. We note that such performances are on-par with the test accuracy of the classical formulation (2), with test accuracy of 99.60% and 78.42% on MNIST and CIFAR10 as reported in Figure 4.

4.3 Insights from $\mathcal{N}\mathcal{C}$ for Improving Network Designs

Finally, we conduct two exploratory experiments to demonstrate the practical benefits of $\mathcal{N}\mathcal{C}$ phenomenon. The universality of $\mathcal{N}\mathcal{C}$ implies that the final classifier (i.e. the L -th layer) of a neural network always converges to a Simplex ETF, which is fully determined up to an arbitrary rotation and happens when $K \leq d$. Thus, based on the understandings of the last-layer features and classifiers, we show that we can substantially improve the cost efficiency on network architecture design without the sacrifice of performance, by (i) fixing the last-layer classifier as a Simplex ETF, and (ii) reducing the feature dimension $d = K$. Here, to demonstrate our method can achieve state-of-the-art performance, it should be noted that for CIFAR10 dataset we also run our experiments on a modified ResNet50 architecture [106] with data augmentation which achieves around 95% test accuracy.

Fixing the Last-layer Classifier as a Simplex ETF. Since we know that the last-layer classifiers and features exhibit $\mathcal{N}\mathcal{C}$, there is no need to train the layer – one can fix the classifier W as a Simplex ETF throughout the training process. In the following, we demonstrate that such a strategy achieves on-par performance with classical fully training protocols and substantially reduces the number of training parameters. More specifically, we train a ResNet18 and fix the weights in the

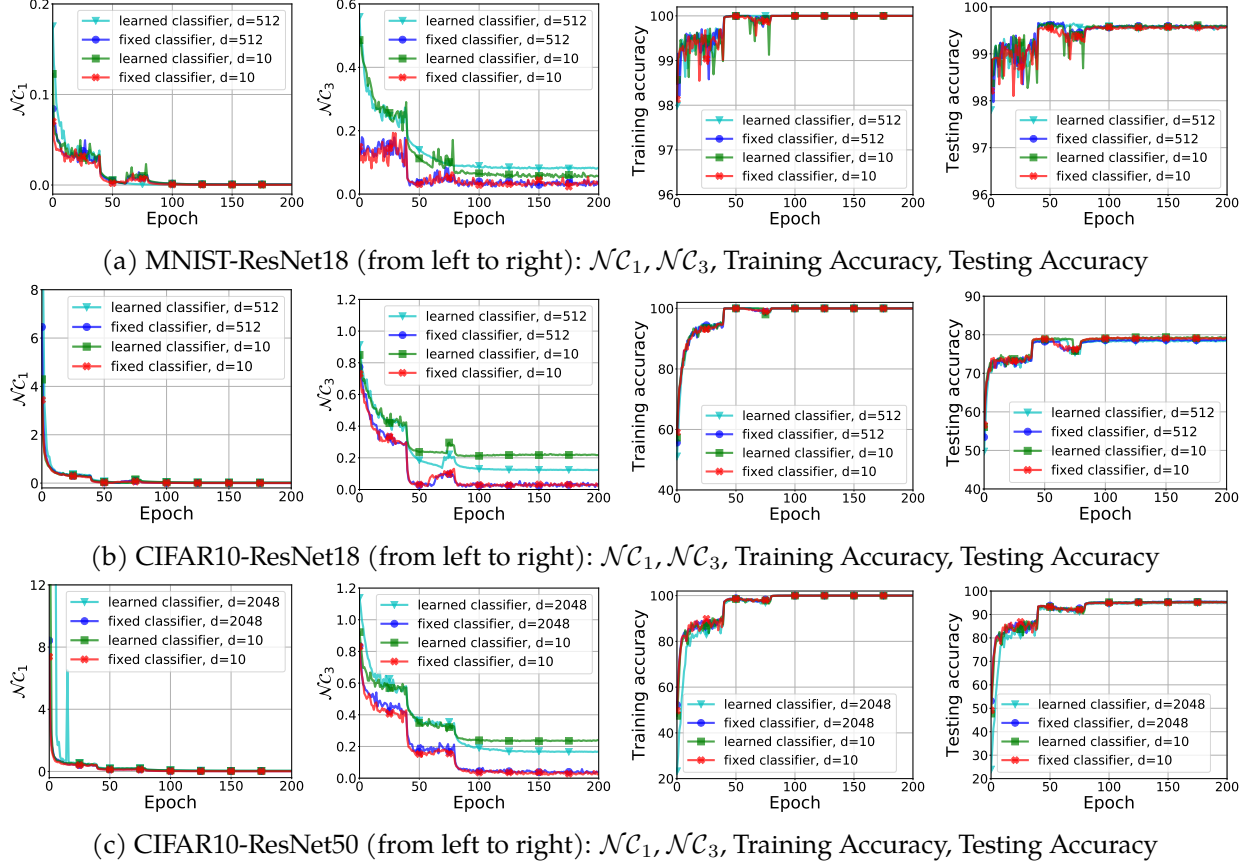


Figure 7: **Comparison of the performances on learned vs. fixed last-layer classifiers.** We compare within-class variation collapse $\mathcal{N}\mathcal{C}_1$, self-duality $\mathcal{N}\mathcal{C}_3$, training accuracy, and test accuracy, on fixed and learned classifier on MNIST-ResNet18 (Top), CIFAR10-ResNet50 (Middle) and CIFAR10-ResNet50 (Bottom). Data augmentation is only used for CIFAR10-ResNet50 (Bottom). All networks are trained by SGD optimizer.

last layer as a Simplex ETF¹⁴ throughout training for MNIST dataset. For CIFAR10 dataset, we train a ResNet18 and also a ResNet50 [106] (so to match the state-of-the-art performance on CIFAR10) and fix the weights in the last layer as a Simplex ETF. We use the data augmentation introduced in [107] during the training phase for ResNet50.¹⁵ We then learn the rest of the parameters of the model¹⁶ using SGD with the same settings as before for both MNIST and CIFAR10 experiments. Figure 7 presents a comparison of learned and fixed classifiers in terms of within-class variation collapse ($\mathcal{N}\mathcal{C}_1$), self-duality ($\mathcal{N}\mathcal{C}_3$), training accuracy, and test accuracy. These results imply that the fixed classifier exhibits the same within-class variation collapse for the feature \mathbf{H} , and achieves the same classification accuracy as the *fully-trained* classifier. On the other hand, fixing the classifier can reduce the number of parameters and the computational complexity for training. The

¹⁴Specifically, we set $\mathbf{W}^\top = \sqrt{\frac{K}{K-1}} \mathbf{P} (\mathbf{I}_K - \frac{1}{K} \mathbf{1}_K \mathbf{1}_K^\top)$ where $\mathbf{P} \in \mathbb{R}^{d \times K}$ contains the first K columns of a $d \times d$ identity matrix, which lifts an $K \times K$ ETF to $d \times K$ matrix.

¹⁵More concretely, the type of data augmentations we use are: (i) Add for 4 pixels on each side for the color-normalized images, (ii) do a random 32×32 crop from the padded images, and then (iii) do a random horizontal flip with probability 0.5. Thus, during the testing phase, the inputs to the network are only 32×32 color-normalized images.

¹⁶For simplicity, we also learn the bias term in the last layer, though our result indicates that it can be set as $\mathbf{W}\bar{\mathbf{h}}$, where \mathbf{W} the classifier and $\bar{\mathbf{h}}$ is the global mean of the features.

number of parameters in the classifier can be significant for tasks with a large number of classes and large feature dimensions. For example, for ImageNet, a dataset with $K = 1000$ classes, fixing the classifier can reduce 8.01%, 11.76%, and 52.56% of total learning parameters for ResNet50, DenseNet169 [19], and ShuffleNet [110], respectively.

Finally, we note that our result also provides a theoretical justification for the work in [111] that fixes the classifier as orthonormal matrices. Indeed, these are close to simplex ETFs, particularly when the number of classes is large. Specifically, for a simplex ETF of size $d \times K$, the inner product between each pair of columns is $-\frac{1}{K-1}$, which is close to 0 (and thus, the matrix is close to an orthonormal matrix) when K is large. Therefore, for a dataset with many classes, such as ImageNet, setting the last layer classifier as an orthonormal matrix or a Simplex ETF is almost identical.

Feature Dimension Reduction for $H \in \mathbb{R}^{d \times nK}$ by Choosing $d = K$.¹⁷ In many classification problems, the practice of deep learning typically uses a feature dimension d that is much larger than the number of classes K . In contrast, \mathcal{NC} implies that there is no need to choose a d that is much larger than the number of classes K . Reducing the dimension d can lead to substantial reductions in memory and computation cost. As shown in Figure 7, we also train all the weights of ResNet18 on MNIST and ResNet50 on CIFAR10 using SGD with $d = K$, respectively. The results demonstrate that \mathcal{NC} persists even when we choose $d = K$, and the network achieves on-par performance with networks of large d , in terms of training and test accuracy. This implies that when the number of classes K is small, we can choose a small feature dimension $d \in O(K)$ instead of using a large universal d to reduce the computation and memory costs for training. By setting $d = K$, this reduces the amount of parameters and hence the memory cost in ResNet18 and ResNet50 by 20.70% and 4.45% respectively.

5 Conclusion

In this work, we have provided an in-depth analysis to demystify the \mathcal{NC} phenomenon, which usually happens during the terminal phase of training deep networks in classification problems. Based on the unconstrained feature model [25–27], we proved that Simplex ETFs are the only global minimizers of the cross-entropy training loss with weight decay and bias. Moreover, we showed that the loss function is a strict saddle function with respect to the last-layer features and classifiers, with no other spurious local minimizers. In contrast to existing landscape analyses for deep neural networks, which mostly focus on the optimization perspective and is often disconnected from practice, our simplified analysis not only characterizes the features are learned in the last layer, but it also explains why they can be efficiently optimized. This provides support for empirical observations in practical deep network architectures. Moreover, the study of last-layer features could have profound implications for optimization, generalization, and robustness of broad interests, which we discuss in the following.

Investigating Deeper Models. Our analysis has so far been focused on the last-layer features, treating them as free optimization variables thanks to the overparameterized nature of the network. A natural extension of these ideas is to further investigate features learned in shallower layers. For example, given that we know that the last-layer classifier \mathbf{W}_L is a Simplex ETF, we can fix the last layer classifier \mathbf{W}_L and study the following 2-layer unconstrained feature model,

$$\psi_{\Theta}(\mathbf{x}) = \mathbf{W}_L \sigma(\mathbf{W}_{L-1} \underbrace{\sigma(\mathbf{W}_{L-2} \cdots \sigma(\mathbf{W}_1 \mathbf{x} + \mathbf{b}_1))}_{\phi'_{\Theta'}(\mathbf{x})} + \mathbf{b}_{L-1}) + \mathbf{b}_L,$$

¹⁷Although Theorem 3.2 only holds for $d > K$, we conjecture it holds for any $d \geq K$ as we have discussed in Section 3.2.

where we treat $\xi = \phi'_{\theta'}(x)$ as an optimization variable. Recent empirical evidence [16, Figure 8] suggests that shallower layers exhibit less severe variability collapse than deeper layers, alas in a progressive manner. Based on the analytical framework that we laid out in this work, it is of interest to investigate the patterns of learned features and the corresponding optimization landscape across shallower layers recursively.

Study of the Relationship Between \mathcal{NC} and Robustness. It has been observed that the \mathcal{NC} phenomenon present during the terminal phase of training improves the adversarial robustness of the learned network [1]. Based on our analytical framework, it would be interesting to theoretically investigate the optimization landscape and representations learned by adversarial training. Indeed, the study of the interplay of the learned features and the final classifier enables precise characterization of the adversarial robustness of the learned model [112]. On the other hand, another line of recent work [33,34] empirically showed and argued that mapping each class to a linearly separable subspace with maximum dimension (instead of collapsing them to a vertex of Simplex ETF) can improve robustness against random data corruptions such as label noise. Further empirical and theoretical investigations are needed to clarify our understandings of potential benefits and full implications of \mathcal{NC} for robustness.

Study of the Relationship Between \mathcal{NC} and Generalization. Our results on the benign landscape of unconstrained feature models imply that \mathcal{NC} is almost universal and agnostic to the choice of optimization algorithms. This seems to be delivering an exciting message that neural networks always converge to a perfect linear classifier in which the peeled-off layers learn maximally separated features and the final layer learns the corresponding maximal margin linear classifier. It is important to note, however, that our result concerns only the training data and does not apply to test data. Since the network is highly overparameterized, there can be infinitely many neural networks with \mathcal{NC} for a particular training dataset with very different generalization. This was also empirically demonstrated in our experiments, showing that different optimization algorithms lead to models that have notably different generalization performances, although all of them exhibit \mathcal{NC} . Therefore, the universality of \mathcal{NC} in fact implies that such a phenomenon cannot fully explain network generalization. A pertinent study of generalization will necessarily require scrutiny into the peeled-off layers, where different optimization methods impose different implicit biases on the learned network parameters.

Study of the Relationship Between \mathcal{NC} and Network Training. While our analysis assumes that the neural network can produce arbitrary features before the final layer due to over-parameterization, one should be reminded that this implicitly requires a good optimization landscape in training the peeled-off layers. On the other hand, it is well-known that deep models can be notoriously difficult to train, due to issues like vanishing and exploding gradients, which leads to complicated landscapes. Efficient optimization techniques for deep learning as of today often rely on residual learning [18], and isometric learning [113], which are crucial for effective training of deep networks beyond a few layers. Pieces of evidence come not only from extensive empirical work that improves network training via enforcing isometry [114–116] but also theoretical work that shows benign optimization landscape of residual and isometric networks [117, 118]. We note that the principles of residual learning and isometric learning, which employs an identity and isometric transformation that preserves distances (and hence, the structure of the data) at each layer, is at odds with \mathcal{NC} , which neglects intrinsic data structures and compresses each class into a vector of Simplex ETF. Resolving this conflict may require us to rethink the cross-entropy loss as a surrogate

for the risk objective and design new objective functions that respect the intrinsic structure of the data [33].

Dealing with a Large Number of Classes $K \gg d$. Finally, it should be noted that our current analysis of the cross-entropy loss for classification focuses on cases where the number of classes, K , is smaller than the feature dimension d . This condition is crucial for showing negative curvatures of the critical saddle points. In many applications, such as recommendation systems [119] and document retrieval [120], the number of classes can be huge and one cannot afford to design a model with feature dimension $d \geq K$. In such cases, our results do not apply; in fact, it is impossible for K features in a d -dimensional space to form a Simplex ETF if $d < K$. This is also the case for contrastive learning [121, 122] in self-supervised feature learning [123], where augmented views of every sample are treated as a “class” so that the total number of classes grows with the size of the dataset. Nonetheless, recent studies in contrastive learning [124, 125] showed that the features learned through the contrastive loss, a variant of cross-entropy loss (3), exhibit properties analogous to \mathcal{NC} . More precisely, samples from the same class are mapped to nearby features, referred to as *alignment*, and feature vectors from different classes are as separated as possible in feature space, referred to as *uniformity*. Hence, the *alignment* and *uniformity* are reminiscent of *variability collapse* and *convergence to Simplex ETF* properties of \mathcal{NC} , respectively, where Simplex ETF can be viewed as an instance of the uniformity property under the special case of $d \geq K$. A precise characterization of the *uniformity* for the case $d \ll K$, in terms of landscape analysis and global optimality, could be an important question for further investigation.

Acknowledgment

ZZ acknowledges support from NSF grant CCF 2008460. XL and QQ acknowledge support from NSF grant DMS 2009752. JS acknowledges support from NSF grant CCF 2007649. We would like to thank Qinqing Zheng (Facebook AI Research), Vardan Papyan (U. Toronto), and Felix Yu (Google Research) for timely pointing us to some important references and valuable feedback on the final draft. We thank Christina Baek (UC Berkeley) and Sam Buchanan (Columbia U.) for fruitful discussions during various stages of the work. We also thank Zhexin Wu (U. Michigan) for proof-reading and pointing out several typos in the draft.

References

- [1] Vardan Papyan, XY Han, and David L Donoho. Prevalence of neural collapse during the terminal phase of deep learning training. *Proceedings of the National Academy of Sciences*, 117(40):24652–24663, 2020.
- [2] Alex Krizhevsky, Ilya Sutskever, and Geoffrey E Hinton. Imagenet classification with deep convolutional neural networks. In *Advances in neural information processing systems*, pages 1097–1105, 2012.
- [3] Yann LeCun, Yoshua Bengio, and Geoffrey Hinton. Deep learning. *nature*, 521(7553):436–444, 2015.
- [4] Ian Goodfellow, Yoshua Bengio, Aaron Courville, and Yoshua Bengio. *Deep learning*, volume 1. MIT press Cambridge, 2016.
- [5] Andrew W Senior, Richard Evans, John Jumper, James Kirkpatrick, Laurent Sifre, Tim Green, Chongli Qin, Augustin Židek, Alexander WR Nelson, Alex Bridgland, et al. Improved protein structure prediction using potentials from deep learning. *Nature*, 577(7792):706–710, 2020.
- [6] Behnam Neyshabur, Ryota Tomioka, and Nathan Srebro. In search of the real inductive bias: On the role of implicit regularization in deep learning. *arXiv preprint arXiv:1412.6614*, 2014.
- [7] Daniel Soudry, Elad Hoffer, Mor Shpigel Nacson, Suriya Gunasekar, and Nathan Srebro. The implicit bias of gradient descent on separable data. *The Journal of Machine Learning Research*, 19(1):2822–2878, 2018.
- [8] Sanjeev Arora, Nadav Cohen, Wei Hu, and Yuping Luo. Implicit regularization in deep matrix factorization. *Advances in Neural Information Processing Systems*, 32, 2019.
- [9] Edward Moroshko, Blake E Woodworth, Suriya Gunasekar, Jason D Lee, Nati Srebro, and Daniel Soudry. Implicit bias in deep linear classification: Initialization scale vs training accuracy. *Advances in Neural Information Processing Systems*, 33, 2020.
- [10] Noam Razin and Nadav Cohen. Implicit regularization in deep learning may not be explainable by norms. *Advances in Neural Information Processing Systems*, 33, 2020.
- [11] Chiyuan Zhang, Samy Bengio, Moritz Hardt, Benjamin Recht, and Oriol Vinyals. Understanding deep learning requires rethinking generalization. *arXiv preprint arXiv:1611.03530*, 2016.
- [12] Mikhail Belkin, Daniel Hsu, Siyuan Ma, and Soumik Mandal. Reconciling modern machine-learning practice and the classical bias–variance trade-off. *Proceedings of the National Academy of Sciences*, 116(32):15849–15854, 2019.
- [13] Song Mei and Andrea Montanari. The generalization error of random features regression: Precise asymptotics and double descent curve. *arXiv preprint arXiv:1908.05355*, 2019.
- [14] Preetum Nakkiran, Gal Kaplun, Yamini Bansal, Tristan Yang, Boaz Barak, and Ilya Sutskever. Deep double descent: Where bigger models and more data hurt. *arXiv preprint arXiv:1912.02292*, 2019.
- [15] Zitong Yang, Yaodong Yu, Chong You, Jacob Steinhardt, and Yi Ma. Rethinking bias-variance trade-off for generalization of neural networks. In *International Conference on Machine Learning*, pages 10767–10777. PMLR, 2020.
- [16] Vardan Papyan. Traces of class/cross-class structure pervade deep learning spectra. *Journal of Machine Learning Research*, 21(252):1–64, 2020.
- [17] Karen Simonyan and Andrew Zisserman. Very deep convolutional networks for large-scale image recognition. *arXiv preprint arXiv:1409.1556*, 2014.
- [18] Kaiming He, Xiangyu Zhang, Shaoqing Ren, and Jian Sun. Deep residual learning for image recognition. In *Proceedings of the IEEE conference on computer vision and pattern recognition*, pages 770–778, 2016.

- [19] Gao Huang, Zhuang Liu, Laurens Van Der Maaten, and Kilian Q Weinberger. Densely connected convolutional networks. In *Proceedings of the IEEE conference on computer vision and pattern recognition*, pages 4700–4708, 2017.
- [20] Yann LeCun, Corinna Cortes, and CJ Burges. Mnist handwritten digit database. at&t labs, 2010.
- [21] Alex Krizhevsky, Geoffrey Hinton, et al. Learning multiple layers of features from tiny images. 2009.
- [22] Jia Deng, Wei Dong, Richard Socher, Li-Jia Li, Kai Li, and Li Fei-Fei. Imagenet: A large-scale hierarchical image database. In *2009 IEEE conference on computer vision and pattern recognition*, pages 248–255. Ieee, 2009.
- [23] John Zarka, Florentin Guth, and Stéphane Mallat. Separation and concentration in deep networks. *arXiv preprint arXiv:2012.10424*, 2020.
- [24] Dustin G Mixon, Hans Parshall, and Jianzong Pi. Neural collapse with unconstrained features. *arXiv preprint arXiv:2011.11619*, 2020.
- [25] Jianfeng Lu and Stefan Steinerberger. Neural collapse with cross-entropy loss. *arXiv preprint arXiv:2012.08465*, 2020.
- [26] E Weinan and Stephan Wojtowytsch. On the emergence of tetrahedral symmetry in the final and penultimate layers of neural network classifiers. *arXiv preprint arXiv:2012.05420*, 2020.
- [27] Cong Fang, Hangfeng He, Qi Long, and Weijie J Su. Layer-peeled model: Toward understanding well-trained deep neural networks. *arXiv preprint arXiv:2101.12699*, 2021.
- [28] Siyuan Ma, Raef Bassily, and Mikhail Belkin. The power of interpolation: Understanding the effectiveness of sgd in modern over-parametrized learning. In *International Conference on Machine Learning*, pages 3325–3334. PMLR, 2018.
- [29] Tengyuan Liang and Alexander Rakhlin. Just interpolate: Kernel “ridgeless” regression can generalize. *The Annals of Statistics*, 48(3):1329 – 1347, 2020.
- [30] Peter L. Bartlett, Philip M. Long, Gábor Lugosi, and Alexander Tsigler. Benign overfitting in linear regression. *Proceedings of the National Academy of Sciences*, 117(48):30063–30070, 2020.
- [31] Zhu Li, Weijie Su, and Dino Sejdinovic. Benign overfitting and noisy features. *arXiv preprint arXiv:2008.02901*, 2020.
- [32] Naftali Tishby and Noga Zaslavsky. Deep learning and the information bottleneck principle. In *2015 IEEE Information Theory Workshop (ITW)*, pages 1–5. IEEE, 2015.
- [33] Yaodong Yu, Kwan Ho Ryan Chan, Chong You, Chaobing Song, and Yi Ma. Learning diverse and discriminative representations via the principle of maximal coding rate reduction. *arXiv preprint arXiv:2006.08558*, 2020.
- [34] Kwan Ho Ryan Chan, Yaodong Yu, Chong You, Haozhi Qi, John Wright, and Yi Ma. Deep networks from the principle of rate reduction. *arXiv preprint arXiv:2010.14765*, 2020.
- [35] Benjamin D Haeffele and René Vidal. Global optimality in tensor factorization, deep learning, and beyond. *arXiv preprint arXiv:1506.07540*, 2015.
- [36] Pierre Baldi and Kurt Hornik. Neural networks and principal component analysis: Learning from examples without local minima. *Neural networks*, 2(1):53–58, 1989.
- [37] Kenji Kawaguchi. Deep learning without poor local minima. *Advances in neural information processing systems*, 29:586–594, 2016.
- [38] Itay Safran and Ohad Shamir. Spurious local minima are common in two-layer relu neural networks. In *International Conference on Machine Learning*, pages 4433–4441. PMLR, 2018.
- [39] Chulhee Yun, Suvrit Sra, and Ali Jadbabaie. Small nonlinearities in activation functions create bad local minima in neural networks. In *International Conference on Learning Representations*, 2018.

- [40] Thomas Laurent and James Brecht. Deep linear networks with arbitrary loss: All local minima are global. In *International conference on machine learning*, pages 2902–2907. PMLR, 2018.
- [41] Maher Nouiehed and Meisam Razaviyayn. Learning deep models: Critical points and local openness. *arXiv preprint arXiv:1803.02968*, 2018.
- [42] Shiyu Liang, Ruoyu Sun, Jason D Lee, and R Srikant. Adding one neuron can eliminate all bad local minima. *Advances in Neural Information Processing Systems*, 2018:4350–4360, 2018.
- [43] Zhihui Zhu, Daniel Soudry, Yonina C Eldar, and Michael B Wakin. The global optimization geometry of shallow linear neural networks. *Journal of Mathematical Imaging and Vision*, pages 1–14, 2019.
- [44] Chulhee Yun, Suvrit Sra, and Ali Jadbabaie. Global optimality conditions for deep neural networks. In *International Conference on Learning Representations*, 2018.
- [45] Mo Zhou, Rong Ge, and Chi Jin. A local convergence theory for mildly over-parameterized two-layer neural network. *arXiv preprint arXiv:2102.02410*, 2021.
- [46] G Cybenko. Approximation by superposition of sigmoidal functions. *Mathematics of Control, Signals and Systems*, 2(4):303–314, 1989.
- [47] Kurt Hornik. Approximation capabilities of multilayer feedforward networks. *Neural networks*, 4(2):251–257, 1991.
- [48] Zhou Lu, Hongming Pu, Feicheng Wang, Zhiqiang Hu, and Liwei Wang. The expressive power of neural networks: a view from the width. In *Proceedings of the 31st International Conference on Neural Information Processing Systems*, pages 6232–6240, 2017.
- [49] Uri Shaham, Alexander Cloninger, and Ronald R Coifman. Provable approximation properties for deep neural networks. *Applied and Computational Harmonic Analysis*, 44(3):537–557, 2018.
- [50] Rong Ge, Furong Huang, Chi Jin, and Yang Yuan. Escaping from saddle points—online stochastic gradient for tensor decomposition. In *Proceedings of The 28th Conference on Learning Theory*, pages 797–842, 2015.
- [51] Ju Sun, Qing Qu, and John Wright. When are nonconvex problems not scary? *arXiv preprint arXiv:1510.06096*, 2015.
- [52] Yuqian Zhang, Qing Qu, and John Wright. From symmetry to geometry: Tractable nonconvex problems. *arXiv preprint arXiv:2007.06753*, 2020.
- [53] Jason D Lee, Max Simchowitz, Michael I Jordan, and Benjamin Recht. Gradient descent only converges to minimizers. In *Conference on learning theory*, pages 1246–1257. PMLR, 2016.
- [54] Michael Elad, Dror Simon, and Aviad Aberdam. Another step toward demystifying deep neural networks. *Proceedings of the National Academy of Sciences*, 117(44):27070–27072, 2020.
- [55] Suriya Gunasekar, Jason Lee, Daniel Soudry, and Nathan Srebro. Implicit bias of gradient descent on linear convolutional networks. In *Advances in Neural Information Processing Systems*, 2018.
- [56] Gauthier Gidel, Francis Bach, and Simon Lacoste-Julien. Implicit regularization of discrete gradient dynamics in linear neural networks. In H. Wallach, H. Larochelle, A. Beygelzimer, F. d’Alché-Buc, E. Fox, and R. Garnett, editors, *Advances in Neural Information Processing Systems*, volume 32, 2019.
- [57] Mor Shpigel Nacson, Jason Lee, Suriya Gunasekar, Pedro Henrique Pamlona Savarese, Nathan Srebro, and Daniel Soudry. Convergence of gradient descent on separable data. In *The 22nd International Conference on Artificial Intelligence and Statistics*, pages 3420–3428. PMLR, 2019.
- [58] Ziwei Ji, Miroslav Dudík, Robert E Schapire, and Matus Telgarsky. Gradient descent follows the regularization path for general losses. In *Conference on Learning Theory*, pages 2109–2136. PMLR, 2020.
- [59] Kaifeng Lyu and Jian Li. Gradient descent maximizes the margin of homogeneous neural networks. In *International Conference on Learning Representations*, 2019.

- [60] Ohad Shamir. Gradient methods never overfit on separable data. *Journal of Machine Learning Research*, 22(85):1–20, 2021.
- [61] Meena Jagadeesan, Ilya Razenshteyn, and Suriya Gunasekar. Inductive bias of multi-channel linear convolutional networks with bounded weight norm. *arXiv preprint arXiv:2102.12238*, 2021.
- [62] Chong You, Zhihui Zhu, Qing Qu, and Yi Ma. Robust recovery via implicit bias of discrepant learning rates for double over-parameterization. In H. Larochelle, M. Ranzato, R. Hadsell, M. F. Balcan, and H. Lin, editors, *Advances in Neural Information Processing Systems*, volume 33, pages 17733–17744. Curran Associates, Inc., 2020.
- [63] John Duchi, Elad Hazan, and Yoram Singer. Adaptive subgradient methods for online learning and stochastic optimization. *Journal of machine learning research*, 12(7), 2011.
- [64] Diederik P Kingma and Jimmy Ba. Adam: A method for stochastic optimization. *arXiv preprint arXiv:1412.6980*, 2014.
- [65] Mor Shpigel Nacson, Nathan Srebro, and Daniel Soudry. Stochastic gradient descent on separable data: Exact convergence with a fixed learning rate. In *The 22nd International Conference on Artificial Intelligence and Statistics*, pages 3051–3059. PMLR, 2019.
- [66] Qian Qian and Xiaoyuan Qian. The implicit bias of adagrad on separable data. *arXiv preprint arXiv:1906.03559*, 2019.
- [67] Suriya Gunasekar, Jason Lee, Daniel Soudry, and Nathan Srebro. Characterizing implicit bias in terms of optimization geometry. In *International Conference on Machine Learning*, pages 1832–1841. PMLR, 2018.
- [68] Ruo-Yu Sun. Optimization for deep learning: An overview. *Journal of the Operations Research Society of China*, 8(2):249–294, 2020.
- [69] Ruoyu Sun, Dawei Li, Shiyu Liang, Tian Ding, and Rayadurgam Srikant. The global landscape of neural networks: An overview. *IEEE Signal Processing Magazine*, 37(5):95–108, 2020.
- [70] Daniel Kunin, Jonathan Bloom, Aleksandrina Goeva, and Cotton Seed. Loss landscapes of regularized linear autoencoders. In *International Conference on Machine Learning*, pages 3560–3569. PMLR, 2019.
- [71] Zeyuan Allen-Zhu, Yuanzhi Li, and Zhao Song. A convergence theory for deep learning via over-parameterization. In *International Conference on Machine Learning*, pages 242–252, 2019.
- [72] Simon Du, Jason Lee, Haochuan Li, Liwei Wang, and Xiyu Zhai. Gradient descent finds global minima of deep neural networks. In *International Conference on Machine Learning*, pages 1675–1685, 2019.
- [73] Arthur Jacot, Clément Hongler, and Franck Gabriel. Neural tangent kernel: Convergence and generalization in neural networks. In *NeurIPS*, 2018.
- [74] Difan Zou, Yuan Cao, Dongruo Zhou, and Quanquan Gu. Gradient descent optimizes over-parameterized deep relu networks. *Machine Learning*, 109(3):467–492, 2020.
- [75] Andrea Montanari and Yiqiao Zhong. The interpolation phase transition in neural networks: Memorization and generalization under lazy training. *arXiv preprint arXiv:2007.12826*, 2020.
- [76] Sam Buchanan, Dar Gilboa, and John Wright. Deep networks and the multiple manifold problem. *arXiv preprint arXiv:2008.11245*, 2020.
- [77] Lénaïc Chizat, Edouard Oyallon, and Francis Bach. On lazy training in differentiable programming. *Advances in Neural Information Processing Systems*, 32:2937–2947, 2019.
- [78] Yuejie Chi, Yue M Lu, and Yuxin Chen. Nonconvex optimization meets low-rank matrix factorization: An overview. *IEEE Transactions on Signal Processing*, 67(20):5239–5269, 2019.
- [79] Marina Danilova, Pavel Dvurechensky, Alexander Gasnikov, Eduard Gorbunov, Sergey Guminov, Dmitry Kamzolov, and Innokentiy Shibaev. Recent theoretical advances in non-convex optimization. *arXiv preprint arXiv:2012.06188*, 2020.

- [80] Qing Qu, Zhihui Zhu, Xiao Li, Manolis C. Tsakiris, John Wright, and René Vidal. Finding the sparsest vectors in a subspace: Theory, algorithms, and applications. *arXiv preprint arXiv:2001.06970*, 2020.
- [81] Chi Jin, Praneeth Netrapalli, Rong Ge, Sham M. Kakade, and Michael I. Jordan. On nonconvex optimization for machine learning: Gradients, stochasticity, and saddle points. *J. ACM*, 68(2), February 2021.
- [82] Tuo Zhao, Zhaoran Wang, and Han Liu. A nonconvex optimization framework for low rank matrix estimation. In *Advances in Neural Information Processing Systems*, pages 559–567, 2015.
- [83] Ju Sun, Qing Qu, and John Wright. Complete dictionary recovery over the sphere I: Overview and the geometric picture. *IEEE Transactions on Information Theory*, 63(2):853–884, 2016.
- [84] Ju Sun, Qing Qu, and John Wright. Complete dictionary recovery over the sphere II: Recovery by Riemannian trust–region method. *IEEE Transactions on Information Theory*, 63(2):853–884, 2017.
- [85] Qiuwei Li, Zhihui Zhu, and Gongguo Tang. The non-convex geometry of low-rank matrix optimization. *Information and Inference: A Journal of the IMA*, 8(1):51–96, 2018.
- [86] Qing Qu, Yuqian Zhang, Yonina Eldar, and John Wright. Convolutional phase retrieval. In *Advances in Neural Information Processing Systems*, pages 6086–6096, 2017.
- [87] Ju Sun, Qing Qu, and John Wright. A geometric analysis of phase retrieval. *Foundations of Computational Mathematics*, 18(5):1131–1198, 2018.
- [88] Zhihui Zhu, Qiuwei Li, Gongguo Tang, and Michael B Wakin. Global optimality in low-rank matrix optimization. *IEEE Transactions on Signal Processing*, 66(13):3614–3628, 2018.
- [89] Xingguo Li, Junwei Lu, Raman Arora, Jarvis Haupt, Han Liu, Zhaoran Wang, and Tuo Zhao. Symmetry, saddle points, and global optimization landscape of nonconvex matrix factorization. *IEEE Transactions on Information Theory*, 65(6):3489–3514, 2019.
- [90] Zhihui Zhu, Qiuwei Li, Xinshuo Yang, Gongguo Tang, and Michael B Wakin. Distributed low-rank matrix factorization with exact consensus. In *Advances in Neural Information Processing Systems*, pages 8422–8432, 2019.
- [91] Qing Qu, Yuexiang Zhai, Xiao Li, Yuqian Zhang, and Zhihui Zhu. Geometric analysis of nonconvex optimization landscapes for overcomplete learning. In *International Conference on Learning Representations*, 2020.
- [92] Qing Qu, Xiao Li, and Zhihui Zhu. Exact recovery of multichannel sparse blind deconvolution via gradient descent. *SIAM Journal on Imaging Sciences*, 13(3):1630–1652, 2020.
- [93] Yenson Lau, Qing Qu, Han-Wen Kuo, Pengcheng Zhou, Yuqian Zhang, and John Wright. Short and sparse deconvolution — a geometric approach. In *International Conference on Learning Representations*, 2020.
- [94] Han-Wen Kuo, Yenson Lau, Yuqian Zhang, and John Wright. Geometry and symmetry in short-and-sparse deconvolution. In *International Conference on Machine Learning*, pages 3570–3580. PMLR, 2019.
- [95] Yuqian Zhang, Han-Wen Kuo, and John Wright. Structured local optima in sparse blind deconvolution. *IEEE Transactions on Information Theory*, 66(1):419–452, 2019.
- [96] Qing Qu, Ju Sun, and John Wright. Finding a sparse vector in a subspace: Linear sparsity using alternating directions. In *Advances in Neural Information Processing Systems*, pages 3401–3409, 2014.
- [97] Vinod Nair and Geoffrey Hinton. Rectified linear units improve restricted boltzmann machines. volume 27, pages 807–814, 2010.
- [98] Sergey Ioffe and Christian Szegedy. Batch normalization: Accelerating deep network training by reducing internal covariate shift. In *ICML*, pages 448–456, 2015.
- [99] Léon Bottou, Frank E Curtis, and Jorge Nocedal. Optimization methods for large-scale machine learning. *Siam Review*, 60(2):223–311, 2018.

- [100] Rong Ge, Jason D Lee, and Tengyu Ma. Matrix completion has no spurious local minimum. *arXiv preprint arXiv:1605.07272*, 2016.
- [101] Srinadh Bhojanapalli, Behnam Neyshabur, and Nathan Srebro. Global optimality of local search for low rank matrix recovery. In *Proceedings of the 30th International Conference on Neural Information Processing Systems*, pages 3880–3888, 2016.
- [102] Rong Ge, Chi Jin, and Yi Zheng. No spurious local minima in nonconvex low rank problems: A unified geometric analysis. In *International Conference on Machine Learning*, pages 1233–1242. PMLR, 2017.
- [103] Qiuwei Li, Zhihui Zhu, and Gongguo Tang. The non-convex geometry of low-rank matrix optimization. *Information and Inference: A Journal of the IMA*, 8(1):51–96, 2019.
- [104] Samuel Burer and Renato DC Monteiro. A nonlinear programming algorithm for solving semidefinite programs via low-rank factorization. *Mathematical Programming*, 95(2):329–357, 2003.
- [105] Yann LeCun. The mnist database of handwritten digits. <http://yann.lecun.com/exdb/mnist/>, 1998.
- [106] kuang Liu, Wei Yang, Yang Peiwen, and Felipe Ducau. Train cifar10 with pytorch. <https://github.com/kuangliu/pytorch-cifar/blob/master/models/resnet.py>.
- [107] Anish Shah, Eashan Kadam, Hena Shah, Sameer Shinde, and Sandip Shingade. Deep residual networks with exponential linear unit. In *Proceedings of the Third International Symposium on Computer Vision and the Internet*, pages 59–65, 2016.
- [108] Raghu Bollapragada, Jorge Nocedal, Dheevatsa Mudigere, Hao-Jun Shi, and Ping Tak Peter Tang. A progressive batching l-bfgs method for machine learning. In *International Conference on Machine Learning*, pages 620–629. PMLR, 2018.
- [109] Yi Ren and Donald Goldfarb. Kronecker-factored quasi-newton methods for convolutional neural networks. *arXiv preprint arXiv:2102.06737*, 2021.
- [110] Xiangyu Zhang, Xinyu Zhou, Mengxiao Lin, and Jian Sun. Shufflenet: An extremely efficient convolutional neural network for mobile devices. In *Proceedings of the IEEE conference on computer vision and pattern recognition*, pages 6848–6856, 2018.
- [111] Elad Hoffer, Itay Hubara, and Daniel Soudry. Fix your classifier: the marginal value of training the last weight layer. In *International Conference on Learning Representations*, 2018.
- [112] Jeremias Sulam, Ramchandran Muthumukar, and Raman Arora. Adversarial robustness of supervised sparse coding. *34th Conference on Neural Information Processing Systems (NeurIPS 2020)*, Vancouver, Canada., 2020.
- [113] Haozhi Qi, Chong You, Xiaolong Wang, Yi Ma, and Jitendra Malik. Deep isometric learning for visual recognition. In Hal Daumé III and Aarti Singh, editors, *Proceedings of the 37th International Conference on Machine Learning*, volume 119 of *Proceedings of Machine Learning Research*, pages 7824–7835. PMLR, 13–18 Jul 2020.
- [114] Lechao Xiao, Yasaman Bahri, Jascha Sohl-Dickstein, Samuel Schoenholz, and Jeffrey Pennington. Dynamical isometry and a mean field theory of cnns: How to train 10,000-layer vanilla convolutional neural networks. In *International Conference on Machine Learning*, pages 5393–5402. PMLR, 2018.
- [115] Weiyang Liu, Rongmei Lin, Zhen Liu, James M. Rehg, Liam Paull, Li Xiong, Le Song, and Adrian Weller. Orthogonal over-parameterized training, 2021.
- [116] Sheng Liu, Xiao Li, Yuexiang Zhai, Chong You, Zhihui Zhu, Carlos Fernandez-Granda, and Qing Qu. Convolutional normalization: Improving deep convolutional network robustness and training, 2021.
- [117] Moritz Hardt and Tengyu Ma. Identity matters in deep learning. *arXiv preprint arXiv:1611.04231*, 2016.
- [118] Wei Hu, Lechao Xiao, and Jeffrey Pennington. Provable benefit of orthogonal initialization in optimizing deep linear networks. In *International Conference on Learning Representations*, 2019.

- [119] Paul Covington, Jay Adams, and Emre Sargin. Deep neural networks for youtube recommendations. In *Proceedings of the 10th ACM conference on recommender systems*, pages 191–198, 2016.
- [120] Wei-Cheng Chang, X Yu Felix, Yin-Wen Chang, Yiming Yang, and Sanjiv Kumar. Pre-training tasks for embedding-based large-scale retrieval. In *International Conference on Learning Representations*, 2019.
- [121] Ting Chen, Simon Kornblith, Mohammad Norouzi, and Geoffrey Hinton. A simple framework for contrastive learning of visual representations. *arXiv preprint arXiv:2002.05709*, 2020.
- [122] Kaiming He, Haoqi Fan, Yuxin Wu, Saining Xie, and Ross Girshick. Momentum contrast for unsupervised visual representation learning. In *Proceedings of the IEEE/CVF Conference on Computer Vision and Pattern Recognition*, pages 9729–9738, 2020.
- [123] Longlong Jing and Yingli Tian. Self-supervised visual feature learning with deep neural networks: A survey. *IEEE Transactions on Pattern Analysis and Machine Intelligence*, 2020.
- [124] Tongzhou Wang and Phillip Isola. Understanding contrastive representation learning through alignment and uniformity on the hypersphere. In *International Conference on Machine Learning*, pages 9929–9939. PMLR, 2020.
- [125] Ting Chen and Lala Li. Intriguing properties of contrastive losses. *arXiv preprint arXiv:2011.02803*, 2020.
- [126] Roger A Horn and Charles R Johnson. *Matrix analysis*. Cambridge University Press, 2012.
- [127] Carlo Ciliberto, Dimitris Stamos, and Massimiliano Pontil. Reexamining low rank matrix factorization for trace norm regularization. *arXiv preprint arXiv:1706.08934*, 2017.
- [128] G Alistair Watson. Characterization of the subdifferential of some matrix norms. *Linear algebra and its applications*, 170:33–45, 1992.
- [129] Benjamin Recht, Maryam Fazel, and Pablo A Parrilo. Guaranteed minimum-rank solutions of linear matrix equations via nuclear norm minimization. *SIAM Review*, 52(3):471–501, 2010.

Appendices

Notations and Organizations. To begin, we first briefly introduce some notations used throughout the appendix. For a scalar function $f(\mathbf{Z})$ with a variable $\mathbf{Z} \in \mathbb{R}^{K \times N}$, its gradient is a $K \times N$ matrix whose (i, j) -th entry is $[\nabla f(\mathbf{Z})]_{ij} = \frac{\partial f(\mathbf{Z})}{\partial z_{ij}}$ for all $i \in [K], j \in [N]$, where z_{ij} represents the (i, j) -th entry of \mathbf{Z} . The Hessian of $f(\mathbf{Z})$ can be viewed as an $KN \times KN$ matrix by vectorizing the matrix \mathbf{Z} . An alternative way to present the Hessian is by a bilinear form defined via $[\nabla^2 f(\mathbf{Z})](\mathbf{A}, \mathbf{B}) = \sum_{i,j,k,\ell} \frac{\partial^2 f(\mathbf{Z})}{\partial z_{ij} \partial z_{k\ell}} a_{ij} b_{k\ell}$ for any $\mathbf{A}, \mathbf{B} \in \mathbb{R}^{K \times N}$, which avoids the procedure of vectorizing the variable \mathbf{Z} . We will use the bilinear form for the Hessian in Section C.

The appendix is organized as follows. In Appendix A, we introduce the basic definitions and inequalities used throughout the appendices. In Appendix B, we provide a detailed proof for Theorem 3.1, showing that the Simplex ETFs are the *only* global minimizers to our regularized cross-entropy loss. Finally, in Appendix C, we present the whole proof for Theorem 3.2 that the function is a strict saddle function and no spurious local minimizers exist, which is one of the major contributions of the work.

A Basics

Definition A.1 (K -Simplex ETF) A standard Simplex ETF is a collection of points in \mathbb{R}^K specified by the columns of

$$\mathbf{M} = \sqrt{\frac{K}{K-1}} \left(\mathbf{I}_K - \frac{1}{K} \mathbf{1}_K \mathbf{1}_K^\top \right),$$

where $\mathbf{I}_K \in \mathbb{R}^{K \times K}$ is the identity matrix, and $\mathbf{1}_K \in \mathbb{R}^K$ is the all ones vector. In the other words, we also have

$$\mathbf{M}^\top \mathbf{M} = \mathbf{M} \mathbf{M}^\top = \frac{K}{K-1} \left(\mathbf{I}_K - \frac{1}{K} \mathbf{1}_K \mathbf{1}_K^\top \right).$$

As in [1, 27], in this paper we consider general Simplex ETF as a collection of points in \mathbb{R}^d specified by the columns of $\sqrt{\frac{K}{K-1}} \mathbf{P} \left(\mathbf{I}_K - \frac{1}{K} \mathbf{1}_K \mathbf{1}_K^\top \right)$, where $\mathbf{P} \in \mathbb{R}^{d \times K}$ ($d \geq K$) is an orthonormal matrix, i.e., $\mathbf{P}^\top \mathbf{P} = \mathbf{I}_K$.

Lemma A.2 (Young's Inequality) Let p, q be positive real numbers satisfying $\frac{1}{p} + \frac{1}{q} = 1$. Then for any $a, b \in \mathbb{R}$, we have

$$|ab| \leq \frac{|a|^p}{p} + \frac{|b|^q}{q},$$

where the equality holds if and only if $|a|^p = |b|^q$. The case $p = q = 2$ is just the AM-GM inequality for a^2, b^2 : $|ab| \leq \frac{1}{2} (a^2 + b^2)$, where the equality holds if and only if $|a| = |b|$.

The following Lemma extends the standard variational form of the nuclear norm.

Lemma A.3 For any fixed $\mathbf{Z} \in \mathbb{R}^{K \times N}$ and $\alpha > 0$, we have

$$\|\mathbf{Z}\|_* = \min_{\mathbf{Z}=\mathbf{W}\mathbf{H}} \frac{1}{2\sqrt{\alpha}} \left(\|\mathbf{W}\|_F^2 + \alpha \|\mathbf{H}\|_F^2 \right). \quad (11)$$

Here, $\|\mathbf{Z}\|_*$ denotes the nuclear norm of \mathbf{Z} :

$$\|\mathbf{Z}\|_* := \sum_{k=1}^{\min\{K,N\}} \sigma_k(\mathbf{Z}) = \text{trace}(\boldsymbol{\Sigma}), \quad \text{with } \mathbf{Z} = \mathbf{U}\boldsymbol{\Sigma}\mathbf{V}^\top,$$

where $\{\sigma_k\}_{k=1}^{\min\{K,N\}}$ denotes the singular values of \mathbf{Z} , and $\mathbf{Z} = \mathbf{U}\boldsymbol{\Sigma}\mathbf{V}^\top$ is the singular value decomposition (SVD) of \mathbf{Z} .

Proof [Proof of Lemma A.3] Let $\mathbf{Z} = \mathbf{U}\boldsymbol{\Sigma}\mathbf{V}^\top$ be the SVD of \mathbf{Z} . First of all, by the facts that $\mathbf{U}^\top\mathbf{U} = \mathbf{I}$, $\mathbf{V}^\top\mathbf{V} = \mathbf{I}$, $\text{trace } \mathbf{A}^\top\mathbf{A} = \|\mathbf{A}\|_F^2$ for any $\mathbf{A} \in \mathbb{R}^{n_1 \times n_2}$, and cyclic permutation invariance of $\text{trace}(\cdot)$, we have

$$\begin{aligned} \|\mathbf{Z}\|_* = \text{trace}(\boldsymbol{\Sigma}) &= \frac{1}{2\sqrt{\alpha}} \text{trace}(\sqrt{\alpha}\mathbf{U}^\top\mathbf{U}\boldsymbol{\Sigma}) + \frac{\sqrt{\alpha}}{2} \text{trace}\left(\frac{1}{\sqrt{\alpha}}\boldsymbol{\Sigma}\mathbf{V}^\top\mathbf{V}\right) \\ &= \frac{1}{2\sqrt{\alpha}} \left(\left\| \alpha^{1/4}\mathbf{U}\boldsymbol{\Sigma}^{1/2} \right\|_F^2 + \alpha \left\| \alpha^{-1/4}\boldsymbol{\Sigma}^{1/2}\mathbf{V}^\top \right\|_F^2 \right). \end{aligned}$$

This implies that there exists some $\mathbf{W} = \alpha^{1/4}\mathbf{U}\boldsymbol{\Sigma}^{1/2}$ and $\mathbf{H} = \alpha^{-1/4}\boldsymbol{\Sigma}^{1/2}\mathbf{V}^\top$, such that $\|\mathbf{Z}\|_* = \frac{1}{2\sqrt{\alpha}} (\|\mathbf{W}\|_F^2 + \alpha\|\mathbf{H}\|_F^2)$. This equality further implies that

$$\|\mathbf{Z}\|_* \geq \min_{\mathbf{Z}=\mathbf{W}\mathbf{H}} \frac{1}{2\sqrt{\alpha}} (\|\mathbf{W}\|_F^2 + \alpha\|\mathbf{H}\|_F^2). \quad (12)$$

On the other hand, for any $\mathbf{W}\mathbf{H} = \mathbf{Z}$, we have

$$\begin{aligned} \|\mathbf{Z}\|_* = \text{trace}(\boldsymbol{\Sigma}) &= \text{trace}(\mathbf{U}^\top\mathbf{Z}\mathbf{V}) = \text{trace}(\mathbf{U}^\top\mathbf{W}\mathbf{H}\mathbf{V}) \\ &\leq \frac{1}{2\sqrt{\alpha}} \left\| \mathbf{U}^\top\mathbf{W} \right\|_F^2 + \frac{\sqrt{\alpha}}{2} \|\mathbf{H}\mathbf{V}\|_F^2 \leq \frac{1}{2\sqrt{\alpha}} (\|\mathbf{W}\|_F^2 + \alpha\|\mathbf{H}\|_F^2), \end{aligned}$$

where the first inequality utilize the Young's inequality in Lemma A.2 that $|\text{trace}(\mathbf{A}\mathbf{B})| \leq \frac{1}{2c} \|\mathbf{A}\|_F^2 + \frac{c}{2} \|\mathbf{B}\|_F^2$ for any $c > 0$ and \mathbf{A}, \mathbf{B} of appropriate dimensions, and the last inequality follows because $\|\mathbf{U}\| = 1$ and $\|\mathbf{V}\| = 1$. Therefore, we have

$$\|\mathbf{Z}\|_* \leq \min_{\mathbf{Z}=\mathbf{W}\mathbf{H}} \frac{1}{2\sqrt{\alpha}} (\|\mathbf{W}\|_F^2 + \alpha\|\mathbf{H}\|_F^2). \quad (13)$$

Combining the results in (12) and (13), we complete the proof. \blacksquare

Lemma A.4 (Theorem 7.2.6 of [126]) Let $\mathbf{A} \in \mathbb{R}^{n \times n}$ be a symmetric positive semidefinite matrix. Then for any fixed $k \in \{2, 3, \dots\}$, there exists a unique real symmetric positive semidefinite matrix \mathbf{B} such that $\mathbf{B}^k = \mathbf{A}$.

B Proof of Theorem 3.1

In this part of appendices, we prove Theorem 3.1 in Section 3 that we restate as follows.

Theorem B.1 (Global Optimality Condition) Assume that the feature dimension d is larger than the number of classes K , i.e., $d > K$. Then any global minimizer $(\mathbf{W}^*, \mathbf{H}^*, \mathbf{b}^*)$ of

$$\min_{\mathbf{W}, \mathbf{H}, \mathbf{b}} f(\mathbf{W}, \mathbf{H}, \mathbf{b}) := g(\mathbf{W}\mathbf{H} + \mathbf{b}\mathbf{1}^\top) + \frac{\lambda_{\mathbf{W}}}{2} \|\mathbf{W}\|_F^2 + \frac{\lambda_{\mathbf{H}}}{2} \|\mathbf{H}\|_F^2 + \frac{\lambda_{\mathbf{b}}}{2} \|\mathbf{b}\|_2^2 \quad (14)$$

with

$$g(\mathbf{W}\mathbf{H} + \mathbf{b}\mathbf{1}^\top) := \frac{1}{N} \sum_{k=1}^K \sum_{i=1}^n \mathcal{L}_{\text{CE}}(\mathbf{W}\mathbf{h}_{k,i} + \mathbf{b}, \mathbf{y}_k), \quad (15)$$

obeys the following

$$\begin{aligned} \|\mathbf{w}^*\|_2 &= \|\mathbf{w}^{*1}\|_2 = \|\mathbf{w}^{*2}\|_2 = \dots = \|\mathbf{w}^{*K}\|_2, \quad \text{and} \quad \mathbf{b}^* = \mathbf{b}^*\mathbf{1}, \\ \mathbf{h}_{k,i}^* &= \sqrt{\frac{\lambda_{\mathbf{W}}}{\lambda_{\mathbf{H}}n}} \mathbf{w}^{*k}, \quad \forall k \in [K], i \in [n], \quad \text{and} \quad \bar{\mathbf{h}}_i^* := \frac{1}{K} \sum_{j=1}^K \mathbf{h}_{j,i}^* = \mathbf{0}, \quad \forall i \in [n], \end{aligned}$$

where either $\mathbf{b}^* = \mathbf{0}$ or $\lambda_{\mathbf{b}} = 0$, and the matrix $\frac{1}{\|\mathbf{w}^*\|_2} \mathbf{W}^{*\top}$ forms a K -simplex ETF defined in Definition A.1 in the sense that

$$\frac{1}{\|\mathbf{w}^*\|_2^2} \mathbf{W}^{*\top} \mathbf{W}^* = \frac{K}{K-1} \left(\mathbf{I}_K - \frac{1}{K} \mathbf{1}_K \mathbf{1}_K^\top \right).$$

B.1 Main Proof

Similar to the proofs in [25, 27], we prove the theorem by directly showing that $f(\mathbf{W}, \mathbf{H}, \mathbf{b}) > f(\mathbf{W}^*, \mathbf{H}^*, \mathbf{b}^*)$ for any $(\mathbf{W}, \mathbf{H}, \mathbf{b})$ not in the form as shown in Theorem B.1.

Proof [Proof of Theorem B.1] First note that the objective function f is *coercive*¹⁸ due to the weight decay regularizers and the fact that the CE loss is always non-negative. This implies that the global minimizer of $f(\mathbf{W}, \mathbf{H}, \mathbf{b})$ in (14) is always finite. By Lemma B.2, we know that any critical point $(\mathbf{W}, \mathbf{H}, \mathbf{b})$ of f in (14) satisfies

$$\mathbf{W}^\top \mathbf{W} = \frac{\lambda_{\mathbf{H}}}{\lambda_{\mathbf{W}}} \mathbf{H} \mathbf{H}^\top.$$

For the rest of the proof, to simplify the notations, let $\|\mathbf{W}\|_F^2 = \rho$, and thus $\|\mathbf{H}\|_F^2 = \frac{\lambda_{\mathbf{W}}}{\lambda_{\mathbf{H}}} \rho$.

We will first provide a lower bound for the cross-entropy term $g(\mathbf{W}\mathbf{H} + \mathbf{b}\mathbf{1}^\top)$ for any \mathbf{W} with energy ρ , and then show that the lower bound is attained if and only if the parameters are in the form described in Theorem B.1. Now, by Lemma B.3, we know that for any $c_1, c_3 > 0$,

$$g(\mathbf{W}\mathbf{H} + \mathbf{b}\mathbf{1}^\top) \geq -\frac{\rho}{(1+c_1)(K-1)} \sqrt{\frac{\lambda_{\mathbf{W}}}{\lambda_{\mathbf{H}}n}} + c_2$$

¹⁸A function $f: \mathbb{R}^n \mapsto \mathbb{R}$ is coercive if $f(\mathbf{x}) \rightarrow +\infty$ as $\|\mathbf{x}\|_2 \rightarrow +\infty$.

with $c_2 = \frac{1}{1+c_1} \log((1+c_1)(K-1)) + \frac{c_1}{1+c_1} \log\left(\frac{1+c_1}{c_1}\right)$. Therefore, we have

$$\begin{aligned} f(\mathbf{W}, \mathbf{H}, \mathbf{b}) &= g(\mathbf{W}\mathbf{H} + \mathbf{b}\mathbf{1}^\top) + \frac{\lambda_{\mathbf{W}}}{2} \|\mathbf{W}\|_F^2 + \frac{\lambda_{\mathbf{H}}}{2} \|\mathbf{H}\|_F^2 + \frac{\lambda_{\mathbf{b}}}{2} \|\mathbf{b}\|_2^2 \\ &\geq \underbrace{-\frac{\rho}{(1+c_1)(K-1)} \sqrt{\frac{\lambda_{\mathbf{W}}}{\lambda_{\mathbf{H}}n}} + c_2 + \lambda_{\mathbf{W}}\rho + \frac{\lambda_{\mathbf{b}}}{2} \|\mathbf{b}\|_2^2}_{\xi(\rho, \lambda_{\mathbf{W}}, \lambda_{\mathbf{H}})} \\ &\geq \xi(\rho, \lambda_{\mathbf{W}}, \lambda_{\mathbf{H}}), \end{aligned}$$

where the last inequality becomes an equality whenever either $\lambda_{\mathbf{b}} = 0$ or $\mathbf{b} = \mathbf{0}$. Furthermore, by Lemma B.4, we know that the inequality $f(\mathbf{W}, \mathbf{H}, \mathbf{b}) \geq \xi(\rho, \lambda_{\mathbf{W}}, \lambda_{\mathbf{H}})$ becomes an equality if and only if $(\mathbf{W}, \mathbf{H}, \mathbf{b})$ satisfy the following

- (a) $\|\mathbf{w}\|_2 = \|\mathbf{w}^1\|_2 = \|\mathbf{w}^2\|_2 = \dots = \|\mathbf{w}^K\|_2$;
- (b) $\mathbf{b} = \mathbf{b}\mathbf{1}$, where either $b = 0$ or $\lambda_{\mathbf{b}} = 0$;
- (c) $\bar{\mathbf{h}}_i := \frac{1}{K} \sum_{j=1}^K \mathbf{h}_{j,i} = \mathbf{0}$, $\forall i \in [n]$, and $\sqrt{\frac{\lambda_{\mathbf{W}}}{\lambda_{\mathbf{H}}n}} \mathbf{w}^k = \mathbf{h}_{k,i}$, $\forall k \in [K]$, $i \in [n]$;
- (d) $\mathbf{W}\mathbf{W}^\top = \frac{\rho}{K-1} (\mathbf{I}_K - \frac{1}{K} \mathbf{1}_K \mathbf{1}_K^\top)$;
- (e) $c_1 = \left[(K-1) \exp\left(-\frac{\rho}{K-1} \sqrt{\frac{\lambda_{\mathbf{W}}}{\lambda_{\mathbf{H}}n}}\right) \right]^{-1}$.

To finish the proof, we only need to show that $\rho = \|\mathbf{W}\|_F^2$ must be finite for any fixed $\lambda_{\mathbf{W}}, \lambda_{\mathbf{H}} > 0$. From (e), we know that $c_1 = \left[(K-1) \exp\left(-\frac{\rho}{K-1} \sqrt{\frac{\lambda_{\mathbf{W}}}{\lambda_{\mathbf{H}}n}}\right) \right]^{-1}$ is an *increasing* function in terms of ρ , and $c_2 = \frac{1}{1+c_1} \log((1+c_1)(K-1)) + \frac{c_1}{1+c_1} \log\left(\frac{1+c_1}{c_1}\right)$ is a *decreasing* function in terms of c_1 . Therefore, we observe the following:

- When $\rho \rightarrow 0$, we have $c_1 \rightarrow \frac{1}{K-1}$ and $c_2 \rightarrow \log K$, so that

$$\lim_{\rho \rightarrow 0} \xi(\rho; \lambda_{\mathbf{W}}, \lambda_{\mathbf{H}}) = \lim_{\rho \rightarrow 0} c_2(\rho) = \log K.$$

- On the other hand, when $\rho \rightarrow +\infty$, $c_1 \rightarrow +\infty$ and $c_2 \rightarrow 0$, so that $\xi(\rho; \lambda_{\mathbf{W}}, \lambda_{\mathbf{H}}) \rightarrow +\infty$ as $\rho \rightarrow +\infty$.

Since $\xi(\rho; \lambda_{\mathbf{W}}, \lambda_{\mathbf{H}})$ is a continuous function of $\rho \in [0, +\infty)$ and $\xi(\rho; \lambda_{\mathbf{W}}, \lambda_{\mathbf{H}}) \rightarrow +\infty$ and $\rho \rightarrow +\infty$, these further imply that $\xi(\rho; \lambda_{\mathbf{W}}, \lambda_{\mathbf{H}})$ achieves its minimum at a finite ρ (see Figure 8 for an example). This finishes the proof. \blacksquare

B.2 Supporting Lemmas

We first characterize the following balance property between \mathbf{W} and \mathbf{H} for any critical point $(\mathbf{W}, \mathbf{H}, \mathbf{b})$ of our loss function:

Lemma B.2 Let $\rho = \|\mathbf{W}\|_F^2$. Any critical point $(\mathbf{W}, \mathbf{H}, \mathbf{b})$ of (14) obeys

$$\mathbf{W}^\top \mathbf{W} = \frac{\lambda_{\mathbf{H}}}{\lambda_{\mathbf{W}}} \mathbf{H}\mathbf{H}^\top \quad \text{and} \quad \rho = \|\mathbf{W}\|_F^2 = \frac{\lambda_{\mathbf{H}}}{\lambda_{\mathbf{W}}} \|\mathbf{H}\|_F^2. \quad (16)$$

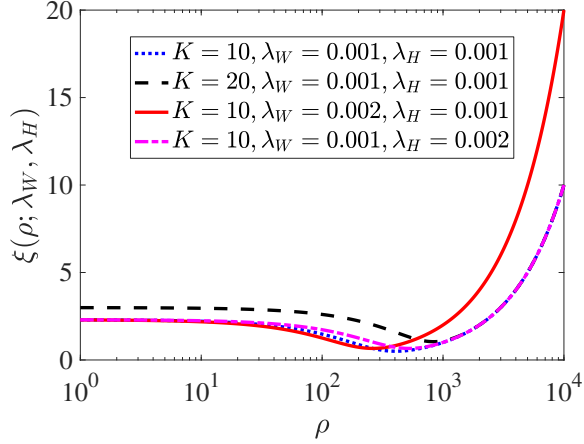


Figure 8: Plot of $\xi(\rho; \lambda_{\mathbf{W}}, \lambda_{\mathbf{H}})$ in terms of ρ for $n = 100$ and different $K, \lambda_{\mathbf{W}}, \lambda_{\mathbf{H}}$.

Proof [Proof of Lemma B.2] By definition, any critical point $(\mathbf{W}, \mathbf{H}, \mathbf{b})$ of (14) satisfies the following:

$$\nabla_{\mathbf{W}} f(\mathbf{W}, \mathbf{H}, \mathbf{b}) = \nabla_{\mathbf{Z}=\mathbf{W}\mathbf{H}} g(\mathbf{W}\mathbf{H} + \mathbf{b}\mathbf{1}^\top) \mathbf{H}^\top + \lambda_{\mathbf{W}} \mathbf{W} = \mathbf{0}, \quad (17)$$

$$\nabla_{\mathbf{H}} f(\mathbf{W}, \mathbf{H}, \mathbf{b}) = \mathbf{W}^\top \nabla_{\mathbf{Z}=\mathbf{W}\mathbf{H}} g(\mathbf{W}\mathbf{H} + \mathbf{b}\mathbf{1}^\top) + \lambda_{\mathbf{H}} \mathbf{H} = \mathbf{0}. \quad (18)$$

Left multiply the first equation by \mathbf{W}^\top on both sides and then right multiply second equation by \mathbf{H}^\top on both sides, it gives

$$\begin{aligned} \mathbf{W}^\top \nabla_{\mathbf{Z}=\mathbf{W}\mathbf{H}} g(\mathbf{W}\mathbf{H} + \mathbf{b}\mathbf{1}^\top) \mathbf{H}^\top &= -\lambda_{\mathbf{W}} \mathbf{W}^\top \mathbf{W}, \\ \mathbf{W}^\top \nabla_{\mathbf{Z}=\mathbf{W}\mathbf{H}} g(\mathbf{W}\mathbf{H} + \mathbf{b}\mathbf{1}^\top) \mathbf{H}^\top &= -\lambda_{\mathbf{H}} \mathbf{H}^\top \mathbf{H}. \end{aligned}$$

Therefore, combining the equations above, we obtain

$$\lambda_{\mathbf{W}} \mathbf{W}^\top \mathbf{W} = \lambda_{\mathbf{H}} \mathbf{H}^\top \mathbf{H}.$$

Moreover, we have

$$\rho = \|\mathbf{W}\|_F^2 = \text{trace}(\mathbf{W}^\top \mathbf{W}) = \frac{\lambda_{\mathbf{H}}}{\lambda_{\mathbf{W}}} \text{trace}(\mathbf{H}^\top \mathbf{H}) = \frac{\lambda_{\mathbf{H}}}{\lambda_{\mathbf{W}}} \|\mathbf{H}\|_F^2,$$

as desired. \blacksquare

Lemma B.3 Let $\mathbf{W} = \begin{bmatrix} (\mathbf{w}^1)^\top \\ \vdots \\ (\mathbf{w}^K)^\top \end{bmatrix} \in \mathbb{R}^{K \times d}$, $\mathbf{H} = [\mathbf{h}_{1,1} \cdots \mathbf{h}_{K,n}] \in \mathbb{R}^{d \times N}$, $N = nK$, and $\rho = \|\mathbf{W}\|_F^2$.

Given $g(\mathbf{W}\mathbf{H} + \mathbf{b}\mathbf{1}^\top)$ defined in (15), for any critical point $(\mathbf{W}, \mathbf{H}, \mathbf{b})$ of (14) and $c_1 > 0$, we have

$$g(\mathbf{W}\mathbf{H} + \mathbf{b}\mathbf{1}^\top) \geq -\frac{\rho}{(1+c_1)(K-1)} \sqrt{\frac{\lambda_{\mathbf{W}}}{\lambda_{\mathbf{H}} n}} + c_2, \quad (19)$$

with $c_2 = \frac{1}{1+c_1} \log((1+c_1)(K-1)) + \frac{c_1}{1+c_1} \log\left(\frac{1+c_1}{c_1}\right)$.

Proof [Proof of Lemma B.3] By Lemma B.5 with $z_{k,i} = \mathbf{W}\mathbf{h}_{k,i} + \mathbf{b}$, since the scalar $c_1 > 0$ can be arbitrary, we choose the same c_1 and c_2 for all $i \in [n]$ and $k \in [K]$, we have the following lower bound for $g(\mathbf{W}\mathbf{H} + \mathbf{b}\mathbf{1}^\top)$ as

$$\begin{aligned}
& (1 + c_1)(K - 1) \left[g(\mathbf{W}\mathbf{H} + \mathbf{b}\mathbf{1}^\top) - c_2 \right] \\
&= (1 + c_1)(K - 1) \left[\frac{1}{N} \sum_{k=1}^K \sum_{i=1}^n \mathcal{L}_{\text{CE}}(\mathbf{W}\mathbf{h}_{k,i} + \mathbf{b}, \mathbf{y}_k) - c_2 \right] \\
&\geq \frac{1}{N} \sum_{k=1}^K \sum_{i=1}^n \left[\sum_{j=1}^K (\mathbf{h}_{k,i}^\top \mathbf{w}^j + b_j) - K (\mathbf{h}_{k,i}^\top \mathbf{w}^k + b_k) \right] \tag{20} \\
&= \frac{1}{N} \sum_{i=1}^n \left[\left(\sum_{k=1}^K \sum_{j=1}^K \mathbf{h}_{k,i}^\top \mathbf{w}^j - K \sum_{k=1}^K \mathbf{h}_{k,i}^\top \mathbf{w}^k \right) + \underbrace{\sum_{k=1}^K \sum_{j=1}^K (b_j - b_k)}_{=0} \right] \\
&= \frac{1}{N} \sum_{i=1}^n \left(\sum_{k=1}^K \sum_{j=1}^K \mathbf{h}_{j,i}^\top \mathbf{w}^k - K \sum_{k=1}^K \mathbf{h}_{k,i}^\top \mathbf{w}^k \right) \\
&= \frac{K}{N} \sum_{i=1}^n \sum_{k=1}^K \left[\left(\frac{1}{K} \sum_{j=1}^K (\mathbf{h}_{j,i} - \mathbf{h}_{k,i}) \right)^\top \mathbf{w}^k \right] = \frac{1}{n} \sum_{i=1}^n \sum_{k=1}^K (\bar{\mathbf{h}}_i - \mathbf{h}_{k,i})^\top \mathbf{w}^k,
\end{aligned}$$

where for the last equality we let $\bar{\mathbf{h}}_i = \frac{1}{K} \sum_{j=1}^K \mathbf{h}_{j,i}$. Furthermore, from the AM-GM inequality in Lemma A.2, we know that for any $\mathbf{u}, \mathbf{v} \in \mathbb{R}^K$ and any $c_3 > 0$,

$$\mathbf{u}^\top \mathbf{v} \leq \frac{c_3}{2} \|\mathbf{u}\|_2^2 + \frac{1}{2c_3} \|\mathbf{v}\|_2^2,$$

where the inequality becomes an equality when $c_3 \mathbf{u} = \mathbf{v}$. Thus, we further have

$$\begin{aligned}
& (1 + c_1)(K - 1) \left[g(\mathbf{W}\mathbf{H} + \mathbf{b}\mathbf{1}^\top) - c_2 \right] \\
&\geq -\frac{c_3}{2} \sum_{k=1}^K \|\mathbf{w}^k\|_2^2 - \frac{1}{2c_3 n} \sum_{i=1}^n \sum_{k=1}^K \|\bar{\mathbf{h}}_i - \mathbf{h}_{k,i}\|_2^2 \\
&= -\frac{c_3}{2} \sum_{k=1}^K \|\mathbf{w}^k\|_2^2 - \frac{1}{2c_3 n} \sum_{i=1}^n \left[\left(\sum_{k=1}^K \|\mathbf{h}_{k,i}\|_2^2 \right) - K \|\bar{\mathbf{h}}_i\|_2^2 \right] \\
&= -\frac{c_3}{2} \|\mathbf{W}\|_F^2 - \frac{1}{2c_3 n} \left(\|\mathbf{H}\|_F^2 - K \sum_{i=1}^n \|\bar{\mathbf{h}}_i\|_2^2 \right),
\end{aligned}$$

where the first inequality becomes an equality if and only if

$$c_3 \mathbf{w}^k = (\mathbf{h}_{k,i} - \bar{\mathbf{h}}_i), \quad \forall k \in [K], i \in [n]. \tag{21}$$

Let $\rho = \|\mathbf{W}\|_F^2$. Now, by using Lemma B.2, we have $\mathbf{W}^\top \mathbf{W} = \frac{\lambda_{\mathbf{H}}}{\lambda_{\mathbf{W}}} \mathbf{H}\mathbf{H}^\top$, so that $\|\mathbf{H}\|_F^2 = \text{trace}(\mathbf{H}\mathbf{H}^\top) = \frac{\lambda_{\mathbf{W}}}{\lambda_{\mathbf{H}}} \text{trace}(\mathbf{W}^\top \mathbf{W}) = \frac{\lambda_{\mathbf{W}}}{\lambda_{\mathbf{H}}} \rho$. Therefore, we have

$$g(\mathbf{W}\mathbf{H} + \mathbf{b}\mathbf{1}^\top) \geq -\frac{\rho}{2(1 + c_1)(K - 1)} \left(c_3 + \frac{\lambda_{\mathbf{W}}}{\lambda_{\mathbf{H}}} \frac{1}{c_3 n} \right) + c_2, \tag{22}$$

as desired. The last inequality achieves its equality if and only if

$$\bar{\mathbf{h}}_i = \mathbf{0}, \quad \forall i \in [n]. \quad (23)$$

Plugging this into (21), we have

$$c_3 \mathbf{w}^k = \mathbf{h}_{k,i} \Rightarrow c_3^2 = \frac{\sum_{i=1}^n \sum_{k=1}^K \|\mathbf{h}_{k,i}\|_2^2}{n \sum_{k=1}^K \|\mathbf{w}^k\|_2^2} = \frac{\|\mathbf{H}\|_F^2}{n \|\mathbf{W}\|_F^2} = \frac{\lambda_{\mathbf{W}}}{n \lambda_{\mathbf{H}}}.$$

This together with the lower bound in (22) gives

$$g(\mathbf{W}\mathbf{H} + \mathbf{b}\mathbf{1}^\top) \geq -\frac{\rho}{(1+c_1)(K-1)} \sqrt{\frac{\lambda_{\mathbf{W}}}{\lambda_{\mathbf{H}}n}} + c_2,$$

as suggested in (19). ■

Next, we show that the lower bound in (19) is attained if and only if $(\mathbf{W}, \mathbf{H}, \mathbf{b})$ satisfies the following conditions.

Lemma B.4 *Under the same assumptions of Lemma B.3, the lower bound in (19) is attained for any critical point $(\mathbf{W}, \mathbf{H}, \mathbf{b})$ of (14) if and only if the following hold*

$$\begin{aligned} \|\mathbf{w}^1\|_2 &= \|\mathbf{w}^2\|_2 = \dots = \|\mathbf{w}^K\|_2, \quad \text{and} \quad \mathbf{b} = \mathbf{b}\mathbf{1}, \\ \bar{\mathbf{h}}_i &:= \frac{1}{K} \sum_{j=1}^K \mathbf{h}_{j,i} = \mathbf{0}, \quad \forall i \in [n], \quad \text{and} \quad \sqrt{\frac{\lambda_{\mathbf{W}}}{\lambda_{\mathbf{H}}n}} \mathbf{w}^k = \mathbf{h}_{k,i}, \quad \forall k \in [K], i \in [n], \\ \mathbf{W}\mathbf{W}^\top &= \frac{\rho}{K-1} \left(\mathbf{I}_K - \frac{1}{K} \mathbf{1}_K \mathbf{1}_K^\top \right), \quad \text{and} \quad c_1 = \left[(K-1) \exp \left(-\frac{\rho}{K-1} \sqrt{\frac{\lambda_{\mathbf{W}}}{\lambda_{\mathbf{H}}n}} \right) \right]^{-1}. \end{aligned}$$

The proof of Lemma B.4 utilizes the conditions in Lemma B.5, and the conditions (21) and (23) during the proof of Lemma B.3.

Proof [Proof of Lemma B.4] From the proof of B.3, if we want to attain the lower bound, we know that we need at least (21) and (23) to hold, which is equivalent to the following:

$$\bar{\mathbf{h}}_i = \frac{1}{K} \sum_{j=1}^K \mathbf{h}_{j,i} = \mathbf{0}, \quad \forall i \in [n], \quad \text{and} \quad \sqrt{\frac{\lambda_{\mathbf{W}}}{\lambda_{\mathbf{H}}n}} \mathbf{w}^k = \mathbf{h}_{k,i}, \quad \forall k \in [K], i \in [n], \quad (24)$$

which further implies that

$$\sum_{k=1}^K \mathbf{w}^k = \mathbf{0}. \quad (25)$$

Next, under the condition (24), if we want (19) to become an equality, we only need (20) to become an equality, which is true if and only if the condition (35) in Lemma B.5 holds for $\mathbf{z}_{k,i} = \mathbf{W}\mathbf{h}_{k,i} + \mathbf{b}$ for all $i \in [n]$ and $k \in [K]$. First, let $[\mathbf{z}_{k,i}]_j = \mathbf{h}_{k,i}^\top \mathbf{w}^j + b_j$, where we have

$$\begin{aligned} \sum_{j=1}^K [\mathbf{z}_{k,i}]_j &= \mathbf{h}_{k,i}^\top \sum_{j=1}^K \mathbf{w}^j + \sum_{j=1}^K b_j = \sqrt{\frac{\lambda_{\mathbf{H}}n}{\lambda_{\mathbf{W}}}} \mathbf{h}_{k,i}^\top \sum_{j=1}^K \mathbf{h}_{j,i} + \sum_{j=1}^K b_j \\ &= \sqrt{\frac{\lambda_{\mathbf{H}}n}{\lambda_{\mathbf{W}}}} K \mathbf{h}_{k,i}^\top \bar{\mathbf{h}}_i + \sum_{j=1}^K b_j = K \bar{b} \end{aligned} \quad (26)$$

with $\bar{b} = \frac{1}{K} \sum_{i=1}^K b_i$, and

$$K[z_{k,i}]_k = K\mathbf{h}_{k,i}^\top \mathbf{w}^k + Kb_k = \sqrt{\frac{\lambda \mathbf{W}}{\lambda_{\mathbf{H}} n}} \left(K \|\mathbf{w}^k\|_2^2 \right) + Kb_k. \quad (27)$$

Based on (26), (27), and (35) from Lemma B.5, we have

$$\begin{aligned} c_1 &= \left[(K-1) \exp \left(\frac{\left(\sum_{j=1}^K [z_{k,i}]_j \right) - K[z_{k,i}]_k}{K-1} \right) \right]^{-1} \\ &= \left[(K-1) \exp \left(\frac{K}{K-1} \left(\bar{b} - \sqrt{\frac{\lambda \mathbf{W}}{\lambda_{\mathbf{H}} n}} \|\mathbf{w}^k\|_2^2 - b_k \right) \right) \right]^{-1}. \end{aligned} \quad (28)$$

Since the scalar $c_1 > 0$ is chosen to be the same for all $k \in [K]$, we have

$$\sqrt{\frac{\lambda \mathbf{W}}{\lambda_{\mathbf{H}} n}} \|\mathbf{w}^k\|_2^2 + b_k = \sqrt{\frac{\lambda \mathbf{W}}{\lambda_{\mathbf{H}} n}} \|\mathbf{w}^\ell\|_2^2 + b_\ell, \quad \forall \ell \neq k. \quad (29)$$

Second, since $[z_{k,i}]_j = [z_{k,i}]_\ell$ for all $\forall j, \ell \neq k, k \in [K]$, from (24) we have

$$\begin{aligned} \mathbf{h}_{k,i}^\top \mathbf{w}^j + b_j &= \mathbf{h}_{k,i}^\top \mathbf{w}^\ell + b_\ell, \quad \forall j, \ell \neq k, k \in [K] \\ \iff \sqrt{\frac{\lambda \mathbf{W}}{\lambda_{\mathbf{H}} n}} (\mathbf{w}^k)^\top \mathbf{w}^j + b_j &= \sqrt{\frac{\lambda \mathbf{W}}{\lambda_{\mathbf{H}} n}} (\mathbf{w}^k)^\top \mathbf{w}^\ell + b_\ell, \quad \forall j, \ell \neq k, k \in [K]. \end{aligned} \quad (30)$$

Based on this and (25), we have

$$\begin{aligned} \sqrt{\frac{\lambda \mathbf{W}}{\lambda_{\mathbf{H}} n}} \|\mathbf{w}^k\|_2^2 + b_k &= -\sqrt{\frac{\lambda \mathbf{W}}{\lambda_{\mathbf{H}} n}} \sum_{j \neq k} (\mathbf{w}^j)^\top \mathbf{w}^k + b_k \\ &= -(K-1) \sqrt{\frac{\lambda \mathbf{W}}{\lambda_{\mathbf{H}} n}} \underbrace{(\mathbf{w}^\ell)^\top \mathbf{w}^k}_{\ell \neq k, \ell \in [K]} + \left(b_k + \sum_{j \neq \ell, k} (b_\ell - b_j) \right) \\ &= -(K-1) \sqrt{\frac{\lambda \mathbf{W}}{\lambda_{\mathbf{H}} n}} (\mathbf{w}^\ell)^\top \mathbf{w}^k + [2b_k + (K-1)b_\ell - K\bar{b}] \end{aligned} \quad (31)$$

for all $\ell \neq k$. Combining (29) and (31), for all $k, \ell \in [K]$ with $k \neq \ell$ we have

$$2b_k + (K-1)b_\ell - K\bar{b} = 2b_\ell + (K-1)b_k - K\bar{b} \iff b_k = b_\ell, \quad \forall k \neq \ell.$$

Therefore, we can write $\mathbf{b} = b\mathbf{1}_K$ for some $b > 0$. Moreover, since $b_k = b_\ell$ for all $k \neq \ell$, (29) and (30), and (31) further imply that

$$\|\mathbf{w}^1\|_2 = \|\mathbf{w}^2\|_2 = \dots = \|\mathbf{w}^K\|_2, \quad \text{and} \quad \|\mathbf{w}^k\|_2^2 = \frac{1}{K} \|\mathbf{W}\|_F^2 = \frac{\rho}{K}, \quad (32)$$

$$(\mathbf{w}^j)^\top \mathbf{w}^k = (\mathbf{w}^\ell)^\top \mathbf{w}^k = -\frac{1}{K-1} \|\mathbf{w}^k\|_2^2 = -\frac{\rho}{K(K-1)}, \quad \forall j, \ell \neq k, k \in [K], \quad (33)$$

where (33) is equivalent to

$$\mathbf{W}\mathbf{W}^\top = \frac{\rho}{K-1} \left(\mathbf{I}_K - \frac{1}{K} \mathbf{1}_K \mathbf{1}_K^\top \right).$$

Finally, plugging the results in (32) and (33) into (28), we have

$$c_1 = \left[(K-1) \exp \left(-\frac{\rho}{K-1} \sqrt{\frac{\lambda_{\mathbf{W}}}{\lambda_{\mathbf{H}} n}} \right) \right]^{-1},$$

as desired. ■

Lemma B.5 *Let $\mathbf{y}_k \in \mathbb{R}^K$ be an one-hot vector with the k th entry equalling 1 for some $k \in [K]$. For any vector $\mathbf{z} \in \mathbb{R}^K$ and $c_1 > 0$, the cross-entropy loss $\mathcal{L}_{\text{CE}}(\mathbf{z}, \mathbf{y}_k)$ with \mathbf{y}_k can be lower bounded by*

$$\mathcal{L}_{\text{CE}}(\mathbf{z}, \mathbf{y}_k) \geq \frac{1}{1+c_1} \frac{\left(\sum_{i=1}^K z_i \right) - K z_k}{K-1} + c_2, \quad (34)$$

where $c_2 = \frac{1}{1+c_1} \log((1+c_1)(K-1)) + \frac{c_1}{1+c_1} \log\left(\frac{1+c_1}{c_1}\right)$. The inequality becomes an equality when

$$z_i = z_j, \quad \forall i, j \neq k, \quad \text{and} \quad c_1 = \left[(K-1) \exp \left(\frac{\left(\sum_{i=1}^K z_i \right) - K z_k}{K-1} \right) \right]^{-1}. \quad (35)$$

Proof [Proof of Lemma B.5] Notice that for any vector $\mathbf{z} \in \mathbb{R}^K$, the cross-entropy loss with \mathbf{y}_k can be lower bounded by

$$\begin{aligned} \mathcal{L}_{\text{CE}}(\mathbf{z}, \mathbf{y}_k) &= \log \left(\frac{\sum_{i=1}^K \exp(z_i)}{\exp(z_k)} \right) = \log \left(1 + \sum_{i \neq k} \exp(z_i - z_k) \right) \\ &\geq \log \left(1 + (K-1) \exp \left(\sum_{i \neq k} \frac{z_i - z_k}{K-1} \right) \right) \\ &= \log \left(1 + (K-1) \exp \left(\frac{\sum_{i=1}^K z_i - K z_k}{K-1} \right) \right) \end{aligned} \quad (36)$$

where the inequality follows from the Jensen's inequality that

$$\sum_{i \neq k} \exp(z_i - z_k) = (K-1) \sum_{i \neq k} \frac{1}{K-1} \exp(z_i - z_k) \geq (K-1) \exp \left(\sum_{i \neq k} \frac{z_i - z_k}{K-1} \right),$$

which achieves the equality only when $z_i = z_j$ for all $i, j \neq k$. Second, by the concavity of the $\log(\cdot)$ function (i.e., $\log(tx + (1-t)x') \geq t \log x + (1-t) \log x'$ for any $x, x' \in \mathbb{R}$ and $t \in [0, 1]$), which

becomes an equality iff $x = x'$, or $t = 0$, or $t = 1$), from (36), for any $c_1 > 0$ we have

$$\begin{aligned}
& \mathcal{L}_{\text{CE}}(\mathbf{z}, \mathbf{y}_k) \\
&= \log \left(\frac{c_1}{1+c_1} \frac{1+c_1}{c_1} + \frac{1}{1+c_1} (1+c_1)(K-1) \exp \left(\frac{\sum_{i=1}^K z_i - K z_k}{K-1} \right) \right) \\
&\geq \frac{1}{1+c_1} \log \left((1+c_1)(K-1) \exp \left(\frac{\sum_{i=1}^K z_i - K z_k}{K-1} \right) \right) + \frac{c_1}{1+c_1} \log \left(\frac{1+c_1}{c_1} \right) \\
&= \frac{1}{1+c_1} \frac{\left(\sum_{i=1}^K z_i \right) - K z_k}{K-1} + \underbrace{\frac{1}{1+c_1} \log((1+c_1)(K-1)) + \frac{c_1}{1+c_1} \log \left(\frac{1+c_1}{c_1} \right)}_{c_2},
\end{aligned}$$

as desired. The last inequality becomes an equality if any only if

$$\frac{1+c_1}{c_1} = (1+c_1)(K-1) \exp \left(\frac{\sum_{i=1}^K z_i - K z_k}{K-1} \right) \quad \text{or} \quad c_1 = 0, \quad \text{or} \quad c_1 = +\infty.$$

However, when $c_1 = 0$ or $c_1 = +\infty$, the equality is trivial. Therefore, we have

$$c_1 = \left[(K-1) \exp \left(\frac{\left(\sum_{i=1}^K z_i \right) - K z_k}{K-1} \right) \right]^{-1},$$

as desired. ■

C Proof of Theorem 3.2

In this part of appendices, we prove Theorem 3.2 in Section 3. In particular, we analyze the global optimization landscape of

$$\min_{\mathbf{W}, \mathbf{H}, \mathbf{b}} f(\mathbf{W}, \mathbf{H}, \mathbf{b}) = \frac{1}{Kn} \sum_{k=1}^K \sum_{i=1}^n \mathcal{L}_{\text{CE}}(\mathbf{W} \mathbf{h}_{k,i} + \mathbf{b}, \mathbf{y}_k) + \frac{\lambda_{\mathbf{W}}}{2} \|\mathbf{W}\|_F^2 + \frac{\lambda_{\mathbf{H}}}{2} \|\mathbf{H}\|_F^2 + \frac{\lambda_{\mathbf{b}}}{2} \|\mathbf{b}\|_2^2,$$

with respect to $\mathbf{W} \in \mathbb{R}^{K \times d}$, $\mathbf{H} = [\mathbf{h}_{1,1} \cdots \mathbf{h}_{K,n}] \in \mathbb{R}^{d \times N}$, and $\mathbf{b} \in \mathbb{R}^K$. We show that the function is a strict saddle function [50–52] in the Euclidean space, that there is no spurious local minimizer and all global minima are corresponding to the form showed in Theorem B.1.

Theorem C.1 (No Spurious Local Minima and Strict Saddle Property) *Assume that the feature dimension d is larger than the number of classes K , i.e., $d > K$. Then the function $f(\mathbf{W}, \mathbf{H}, \mathbf{b})$ in (14) is a strict saddle function with no spurious local minimum:*

- Any local minimizer of (14) is a global minimum of the form shown in Theorem B.1.
- Any critical point of (14) that is not a local minimum has at least one negative curvature direction, i.e., the Hessian $\nabla^2 f(\mathbf{W}, \mathbf{H}, \mathbf{b})$ at this point has at least one negative eigenvalue

$$\lambda_i(\nabla^2 f(\mathbf{W}, \mathbf{H}, \mathbf{b})) < 0.$$

C.1 Main Proof

Proof [Proof of Theorem C.1] The main idea of proving Theorem 3.2 is to first connect the problem (14) to its corresponding convex counterpart, so that we can obtain the global optimality conditions for the original problem (14) based on the convex counterpart. Finally, we characterize the properties of all the critical points based on the optimality condition. We describe this in more detail as follows.

Connection of (14) to a Convex Program. Let $\mathbf{Z} = \mathbf{H}\mathbf{W} \in \mathbb{R}^{K \times N}$ with $N = nK$ and $\alpha = \frac{\lambda_H}{\lambda_W}$. By Lemma A.3, we know that

$$\begin{aligned} \min_{\mathbf{H}\mathbf{W}=\mathbf{Z}} \frac{\lambda_W}{2} \|\mathbf{W}\|_F^2 + \frac{\lambda_H}{2} \|\mathbf{H}\|_F^2 &= \sqrt{\lambda_W \lambda_H} \min_{\mathbf{H}\mathbf{W}=\mathbf{Z}} \frac{1}{2\sqrt{\alpha}} \left(\|\mathbf{W}\|_F^2 + \alpha \|\mathbf{H}\|_F^2 \right) \\ &= \sqrt{\lambda_W \lambda_H} \|\mathbf{Z}\|_*. \end{aligned}$$

Thus, we can relate the bilinear factorized problem (14) to a convex problem in terms of \mathbf{Z} and \mathbf{b} as follows

$$\min_{\mathbf{Z} \in \mathbb{R}^{K \times N}, \mathbf{b} \in \mathbb{R}^K} \tilde{f}(\mathbf{Z}, \mathbf{b}) := g(\mathbf{Z} + \mathbf{b}\mathbf{1}^\top) + \sqrt{\lambda_W \lambda_H} \|\mathbf{Z}\|_* + \frac{\lambda_b}{2} \|\mathbf{b}\|_2^2. \quad (37)$$

Similar to the idea in [35,88,103,127], we will characterize the critical points of (14) by establishing a connection to the optimality condition of the convex problem (37). Towards this goal, we first show the global minimum of the convex program (37) provides a lower bound for the original problem (4). More specifically, in Lemma C.2 we can show that for any global minimizer $(\mathbf{Z}_*, \mathbf{b}_*)$ of \tilde{f} satisfies

$$\tilde{f}(\mathbf{Z}_*, \mathbf{b}_*) \leq f(\mathbf{W}, \mathbf{H}, \mathbf{b}), \quad \forall \mathbf{W} \in \mathbb{R}^{K \times d}, \mathbf{H} \in \mathbb{R}^{d \times N}, \mathbf{b} \in \mathbb{R}^K. \quad (38)$$

Characterizing the Optimality Condition of (14) Based on the Convex Program (37). Next, we characterize the optimality condition of our nonconvex problem (14), based on the relationship to its convex counterpart (37). Specifically, Lemma C.3 showed that any critical point (\mathbf{Z}, \mathbf{b}) of (37) is characterized by the following necessary and sufficient condition

$$\begin{aligned} \nabla g(\mathbf{Z} + \mathbf{b}\mathbf{1}^\top) &\in -\sqrt{\lambda_W \lambda_H} \partial \|\mathbf{Z}\|_*, \\ \sum_{i=1}^N [\nabla g(\mathbf{Z} + \mathbf{b}\mathbf{1}^\top)]_i + \lambda_b \mathbf{b} &= \mathbf{0}, \end{aligned} \quad (39)$$

where $[\nabla g(\mathbf{Z} + \mathbf{b}\mathbf{1}^\top)]_i$ represents the i -th column in $\nabla g(\mathbf{Z} + \mathbf{b}\mathbf{1}^\top)$. By Lemma C.4, we can transfer the optimality condition from convex to the nonconvex problem (14). More specifically, any critical point $(\mathbf{W}, \mathbf{H}, \mathbf{b})$ of (14) satisfies

$$\left\| \nabla g(\mathbf{W}\mathbf{H} + \mathbf{b}\mathbf{1}^\top) \right\| \leq \sqrt{\lambda_W \lambda_H},$$

then (\mathbf{Z}, \mathbf{b}) with $\mathbf{Z} = \mathbf{W}\mathbf{H}$ satisfies all the conditions in (39). Combining with (38), Lemma C.4 showed that $(\mathbf{W}, \mathbf{H}, \mathbf{b})$ is a global solution of the nonconvex problem (14).

Proving No Spurious Local Minima and Strict Saddle Property. Now we turn to prove the strict saddle property and that there are no spurious local minima by characterizing the properties for all the critical points of (14). Denote the set of critical points of $f(\mathbf{W}, \mathbf{H}, \mathbf{b})$ by

$$\mathcal{C} := \left\{ \mathbf{W} \in \mathbb{R}^{K \times d}, \mathbf{H} \in \mathbb{R}^{d \times N}, \mathbf{b} \in \mathbb{R}^K \mid \nabla f(\mathbf{W}, \mathbf{H}, \mathbf{b}) = \mathbf{0} \right\}.$$

To proceed, we separate the set \mathcal{C} into two disjoint subsets

$$\begin{aligned} \mathcal{C}_1 &:= \mathcal{C} \cap \left\{ \mathbf{W} \in \mathbb{R}^{K \times d}, \mathbf{H} \in \mathbb{R}^{d \times N}, \mathbf{b} \in \mathbb{R}^K \mid \left\| \nabla g(\mathbf{W}\mathbf{H} + \mathbf{b}\mathbf{1}^\top) \right\| \leq \sqrt{\lambda_{\mathbf{W}}\lambda_{\mathbf{H}}} \right\}, \\ \mathcal{C}_2 &:= \mathcal{C} \cap \left\{ \mathbf{W} \in \mathbb{R}^{K \times d}, \mathbf{H} \in \mathbb{R}^{d \times N}, \mathbf{b} \in \mathbb{R}^K \mid \left\| \nabla g(\mathbf{W}\mathbf{H} + \mathbf{b}\mathbf{1}^\top) \right\| > \sqrt{\lambda_{\mathbf{W}}\lambda_{\mathbf{H}}} \right\}, \end{aligned}$$

satisfying $\mathcal{C} = \mathcal{C}_1 \cup \mathcal{C}_2$. By Lemma C.4, we already know that any $(\mathbf{W}, \mathbf{H}, \mathbf{b}) \in \mathcal{C}_1$ is a global optimal solution of $f(\mathbf{W}, \mathbf{H}, \mathbf{b})$ in (14). If we can show that any critical point in \mathcal{C}_2 possesses negative curvatures (i.e., the Hessian at $(\mathbf{W}, \mathbf{H}, \mathbf{b})$ has at least one negative eigenvalue), then we prove that there is no spurious local minima as well as strict saddle property.

Thus, the remaining part is to show any point in \mathcal{C}_2 possesses negative curvatures. We will find a direction Δ along which the Hessian has a strictly negative curvature for this point. Towards that goal, for any $\Delta = (\Delta_{\mathbf{W}}, \Delta_{\mathbf{H}}, \Delta_{\mathbf{b}})$, we first compute the Hessian bilinear form of $f(\mathbf{W}, \mathbf{H}, \mathbf{b})$ along the direction Δ by

$$\begin{aligned} &\nabla^2 f(\mathbf{W}, \mathbf{H}, \mathbf{b})[\Delta, \Delta] \\ &= \nabla^2 g(\mathbf{W}\mathbf{H} + \mathbf{b}\mathbf{1}^\top) \left[\mathbf{W}\Delta_{\mathbf{H}} + \Delta_{\mathbf{W}}\mathbf{H} + \Delta_{\mathbf{b}}\mathbf{1}^\top, \mathbf{W}\Delta_{\mathbf{H}} + \Delta_{\mathbf{W}}\mathbf{H} + \Delta_{\mathbf{b}}\mathbf{1}^\top \right] \\ &\quad + 2 \left\langle \nabla g(\mathbf{W}\mathbf{H} + \mathbf{b}\mathbf{1}^\top), \Delta_{\mathbf{W}}\Delta_{\mathbf{H}} \right\rangle + \lambda_{\mathbf{W}} \|\Delta_{\mathbf{W}}\|_F^2 + \lambda_{\mathbf{H}} \|\Delta_{\mathbf{H}}\|_F^2 + \lambda_{\mathbf{b}} \|\Delta_{\mathbf{b}}\|_2^2. \end{aligned} \quad (40)$$

We now utilize the property that $\|\nabla g(\mathbf{W}\mathbf{H} + \mathbf{b}\mathbf{1}^\top)\| > \sqrt{\lambda_{\mathbf{W}}\lambda_{\mathbf{H}}}$ for any $(\mathbf{W}, \mathbf{H}, \mathbf{b}) \in \mathcal{C}_2$ to construct a negative curvature direction. Let \mathbf{u} and \mathbf{v} be the left and right singular vectors corresponding to the largest singular value $\sigma_1(\nabla^2 g(\mathbf{W}\mathbf{H} + \mathbf{b}\mathbf{1}^\top))$ of $\nabla^2 g(\mathbf{W}\mathbf{H} + \mathbf{b}\mathbf{1}^\top)$, which is larger than $\sqrt{\lambda_{\mathbf{W}}\lambda_{\mathbf{H}}}$ by our assumption.

Since $d > K$ and $\mathbf{W} \in \mathbb{R}^{K \times d}$, there exists a nonzero $\mathbf{a} \in \mathbb{R}^d$ in the null space of \mathbf{W} , i.e., $\mathbf{W}\mathbf{a} = \mathbf{0}$. Furthermore, by Lemma B.2, we know that

$$\mathbf{W}^\top \mathbf{W} = \sqrt{\frac{\lambda_{\mathbf{H}}}{\lambda_{\mathbf{W}}}} \mathbf{H}\mathbf{H}^\top \implies \mathbf{H}^\top \mathbf{a} = \mathbf{0}.$$

We now construct the negative curvature direction as

$$\Delta = (\Delta_{\mathbf{W}}, \Delta_{\mathbf{H}}, \Delta_{\mathbf{b}}) = \left(\left(\frac{\lambda_{\mathbf{H}}}{\lambda_{\mathbf{W}}} \right)^{1/4} \mathbf{u}\mathbf{a}^\top, - \left(\frac{\lambda_{\mathbf{H}}}{\lambda_{\mathbf{W}}} \right)^{-1/4} \mathbf{a}\mathbf{v}^\top, \mathbf{0} \right)$$

so that the term $\langle \nabla g(\mathbf{W}\mathbf{H} + \mathbf{b}\mathbf{1}^\top), \Delta_{\mathbf{W}}\Delta_{\mathbf{H}} \rangle$ is small enough to create a negative curvature. Since $\mathbf{W}\mathbf{a} = \mathbf{0}$, $\mathbf{a}^\top \mathbf{H} = \mathbf{0}$, and $\Delta_{\mathbf{b}} = \mathbf{0}$, we have

$$\mathbf{W}\Delta_{\mathbf{H}} + \Delta_{\mathbf{W}}\mathbf{H} + \Delta_{\mathbf{b}}\mathbf{1}^\top = - \left(\frac{\lambda_{\mathbf{H}}}{\lambda_{\mathbf{W}}} \right)^{-1/4} \mathbf{W}\mathbf{a}\mathbf{v}^\top + \left(\frac{\lambda_{\mathbf{H}}}{\lambda_{\mathbf{W}}} \right)^{1/4} \mathbf{u}\mathbf{a}^\top \mathbf{H} = \mathbf{0},$$

so that $\nabla^2 g(\mathbf{W}\mathbf{H} + \mathbf{b}\mathbf{1}^\top) [\mathbf{W}\Delta_{\mathbf{H}} + \Delta_{\mathbf{W}}\mathbf{H} + \Delta_{\mathbf{b}}\mathbf{1}^\top, \mathbf{W}\Delta_{\mathbf{H}} + \Delta_{\mathbf{W}}\mathbf{H} + \Delta_{\mathbf{b}}\mathbf{1}^\top] = 0$. Thus, combining the results above with (40), we obtain the following

$$\begin{aligned} & \nabla f(\mathbf{W}, \mathbf{H}, \mathbf{b})[\Delta, \Delta] \\ &= 2 \left\langle \nabla g(\mathbf{W}\mathbf{H} + \mathbf{b}\mathbf{1}^\top), \Delta_{\mathbf{W}}\Delta_{\mathbf{H}} \right\rangle + \lambda_{\mathbf{W}} \|\Delta_{\mathbf{W}}\|_F^2 + \lambda_{\mathbf{H}} \|\Delta_{\mathbf{H}}\|_F^2 \\ &= -2 \|\mathbf{a}\|_2^2 \left\langle \nabla g(\mathbf{W}\mathbf{H} + \mathbf{b}\mathbf{1}^\top), \mathbf{u}\mathbf{v}^\top \right\rangle + 2\sqrt{\lambda_{\mathbf{W}}\lambda_{\mathbf{H}}} \|\mathbf{a}\|_2^2 \\ &= -2 \|\mathbf{a}\|_2^2 \left(\left\| \nabla g(\mathbf{W}\mathbf{H} + \mathbf{b}\mathbf{1}^\top) \right\| - \sqrt{\lambda_{\mathbf{W}}\lambda_{\mathbf{H}}} \right) < 0, \end{aligned}$$

where the last inequality is based on the fact that $(\mathbf{W}, \mathbf{H}, \mathbf{b}) \in \mathcal{C}_2$ so that $\left\| \nabla g(\mathbf{W}\mathbf{H} + \mathbf{b}\mathbf{1}^\top) \right\| > \sqrt{\lambda_{\mathbf{W}}\lambda_{\mathbf{H}}}$. Therefore, any $(\mathbf{W}, \mathbf{H}, \mathbf{b}) \in \mathcal{C}_2$ possesses at least one negative curvature direction. This completes our proof of Theorem C.1. \blacksquare

C.2 Supporting Lemmas

Lemma C.2 *If $(\mathbf{Z}^*, \mathbf{b}^*)$ is a global minimizer of*

$$\min_{\mathbf{Z} \in \mathbb{R}^{K \times N}, \mathbf{b} \in \mathbb{R}^K} \tilde{f}(\mathbf{Z}, \mathbf{b}) := g(\mathbf{Z} + \mathbf{b}\mathbf{1}^\top) + \sqrt{\lambda_{\mathbf{W}}\lambda_{\mathbf{H}}} \|\mathbf{Z}\|_* + \frac{\lambda_{\mathbf{b}}}{2} \|\mathbf{b}\|_2^2.$$

introduced in (37), then $\tilde{f}(\mathbf{Z}^, \mathbf{b}^*) \leq f(\mathbf{W}, \mathbf{H}, \mathbf{b})$ for all $\mathbf{W} \in \mathbb{R}^{K \times d}$, $\mathbf{H} \in \mathbb{R}^{d \times N}$, $\mathbf{b} \in \mathbb{R}^K$.*

Proof [Proof of Lemma C.2] Suppose $(\mathbf{Z}^*, \mathbf{b}^*)$ is a global minimum of $\tilde{f}(\mathbf{Z}, \mathbf{b})$. Then by Theorem A.3, we have

$$\begin{aligned} \tilde{f}(\mathbf{Z}^*, \mathbf{b}^*) &= \min_{\mathbf{Z}, \mathbf{b}} g(\mathbf{Z} + \mathbf{b}\mathbf{1}^\top) + \sqrt{\lambda_{\mathbf{W}}\lambda_{\mathbf{H}}} \|\mathbf{Z}\|_* + \frac{\lambda_{\mathbf{b}}}{2} \|\mathbf{b}\|_2^2 \\ &= \min_{\mathbf{Z}, \mathbf{b}} g(\mathbf{Z} + \mathbf{b}\mathbf{1}^\top) + \min_{\mathbf{W}\mathbf{H}=\mathbf{Z}} \left(\frac{\lambda_{\mathbf{W}}}{2} \|\mathbf{W}\|_F^2 + \frac{\lambda_{\mathbf{H}}}{2} \|\mathbf{H}\|_F^2 \right) + \frac{\lambda_{\mathbf{b}}}{2} \|\mathbf{b}\|_2^2 \\ &\leq \min_{\mathbf{W}, \mathbf{H}, \mathbf{Z}, \mathbf{b}, \mathbf{Z}=\mathbf{W}\mathbf{H}} g(\mathbf{W}\mathbf{H} + \mathbf{b}\mathbf{1}^\top) + \frac{\lambda_{\mathbf{W}}}{2} \|\mathbf{W}\|_F^2 + \frac{\lambda_{\mathbf{H}}}{2} \|\mathbf{H}\|_F^2 + \frac{\lambda_{\mathbf{b}}}{2} \|\mathbf{b}\|_2^2. \end{aligned}$$

Thus, we have

$$\tilde{f}(\mathbf{Z}^*, \mathbf{b}^*) \leq \min_{\mathbf{W} \in \mathbb{R}^{K \times d}, \mathbf{H} \in \mathbb{R}^{d \times N}, \mathbf{b} \in \mathbb{R}^K} f(\mathbf{W}, \mathbf{H}, \mathbf{b})$$

as desired. \blacksquare

Lemma C.3 (Optimality Condition for the Convex Program (37)) *Consider the following convex program in (37) that we rewrite as follows*

$$\min_{\mathbf{Z} \in \mathbb{R}^{K \times N}, \mathbf{b} \in \mathbb{R}^K} \tilde{f}(\mathbf{Z}, \mathbf{b}) := g(\mathbf{Z} + \mathbf{b}\mathbf{1}^\top) + \sqrt{\lambda_{\mathbf{W}}\lambda_{\mathbf{H}}} \|\mathbf{Z}\|_* + \frac{\lambda_{\mathbf{b}}}{2} \|\mathbf{b}\|_2^2.$$

Then the necessary and sufficient condition for (\mathbf{Z}, \mathbf{b}) being the global solution of (37) is

$$\begin{aligned} \nabla g(\mathbf{Z} + \mathbf{b}\mathbf{1}^\top)\mathbf{V} &= -\sqrt{\lambda_{\mathbf{W}}\lambda_{\mathbf{H}}}\mathbf{U}, \quad \nabla g(\mathbf{Z} + \mathbf{b}\mathbf{1}^\top)^\top\mathbf{U} = -\sqrt{\lambda_{\mathbf{W}}\lambda_{\mathbf{H}}}\mathbf{V}, \\ \left\| \nabla g(\mathbf{Z} + \mathbf{b}\mathbf{1}^\top) \right\| &\leq \sqrt{\lambda_{\mathbf{W}}\lambda_{\mathbf{H}}}, \quad \text{and} \quad \sum_{i=1}^N [\nabla g(\mathbf{Z} + \mathbf{b}\mathbf{1}^\top)]_i + \lambda_{\mathbf{b}}\mathbf{b} = \mathbf{0}, \end{aligned} \tag{41}$$

where \mathbf{U} and \mathbf{V} are the left and right singular value matrices of \mathbf{Z} , i.e., $\mathbf{Z} = \mathbf{U}\Sigma\mathbf{V}^\top$.

Proof [Proof of Lemma C.3] Standard convex optimization theory asserts that any critical point (\mathbf{Z}, \mathbf{b}) of (37) is global, where the optimality is characterized by the following necessary and sufficient condition

$$\begin{aligned} \nabla g(\mathbf{Z} + \mathbf{b}\mathbf{1}^\top) &\in -\sqrt{\lambda_{\mathbf{W}}\lambda_{\mathbf{H}}}\partial\|\mathbf{Z}\|_*, \\ \sum_{i=1}^N [\nabla g(\mathbf{Z} + \mathbf{b}\mathbf{1}^\top)]_i + \lambda_{\mathbf{b}}\mathbf{b} &= \mathbf{0}, \end{aligned} \quad (42)$$

where $[\nabla g(\mathbf{Z} + \mathbf{b}\mathbf{1}^\top)]_i$ represents the i -th column in $\nabla g(\mathbf{Z} + \mathbf{b}\mathbf{1}^\top)$, and $\partial\|\mathbf{Z}\|_*$ denotes the subdifferential of the convex nuclear norm $\|\mathbf{Z}\|_*$ evaluated at \mathbf{Z} . By its definition, we have

$$\partial\|\mathbf{Z}\|_* := \left\{ \mathbf{D} \in \mathbb{R}^{K \times N} \mid \|\mathbf{G}\|_* \geq \|\mathbf{Z}\|_* + \langle \mathbf{G} - \mathbf{Z}, \mathbf{D} \rangle, \mathbf{G} \in \mathbb{R}^{K \times N} \right\},$$

where for nuclear norm, the previous work [128, 129] showed that based on the projection onto the column space and row space via the SVD of $\mathbf{Z} = \mathbf{U}\mathbf{\Sigma}\mathbf{V}^\top$, this is equivalent to

$$\partial\|\mathbf{Z}\|_* = \left\{ \mathbf{U}\mathbf{V}^\top + \mathbf{W}, \mathbf{W} \in \mathbb{R}^{K \times N} \mid \mathbf{U}^\top \mathbf{W} = \mathbf{0}, \mathbf{W}\mathbf{V} = \mathbf{0}, \|\mathbf{W}\| \leq 1 \right\},$$

where \mathbf{U} and \mathbf{V} are the left and right singular value matrices of \mathbf{Z} . Using the result above, we can now rewrite the optimality condition in (42) as suggested in Lemma C.3. ■

Lemma C.4 (Optimality Condition for the Nonconvex Program (14)) *If a critical point $(\mathbf{W}, \mathbf{H}, \mathbf{b})$ of (14) satisfies*

$$\left\| \nabla g(\mathbf{W}\mathbf{H} + \mathbf{b}\mathbf{1}^\top) \right\| \leq \sqrt{\lambda_{\mathbf{W}}\lambda_{\mathbf{H}}}, \quad (43)$$

then it is a global minimum of (14).

Proof [Proof of Lemma C.4] Suppose $(\mathbf{W}^*, \mathbf{H}^*, \mathbf{b}^*)$ is a critical point of (14) satisfying (43), we will show that $(\mathbf{Z}^*, \mathbf{b}^*)$ with $\mathbf{Z}^* = \mathbf{W}^*\mathbf{H}^*$ is a global minimizer of (37) by showing that $(\mathbf{W}^*\mathbf{H}^*, \mathbf{b}^*)$ satisfies the optimality condition for the convex program in (41) (Lemma C.3). First of all, it is easy to check that

$$\begin{aligned} \nabla_b f(\mathbf{W}^*, \mathbf{H}^*, \mathbf{b}^*) &= \sum_{i=1}^N [\nabla g(\mathbf{W}^*\mathbf{H}^* + \mathbf{b}^*\mathbf{1}^\top)]_i + \lambda_{\mathbf{b}}\mathbf{b}^* = \mathbf{0} \\ \implies \sum_{i=1}^N [\nabla g(\mathbf{Z}^* + \mathbf{b}^*\mathbf{1}^\top)]_i + \lambda_{\mathbf{b}}\mathbf{b}^* &= \mathbf{0}. \end{aligned}$$

Second, let $\mathbf{Z}^* = \mathbf{W}^*\mathbf{H}^* = \mathbf{U}\mathbf{\Sigma}\mathbf{V}^\top$ be the compact SVD of $\mathbf{Z}^* = \mathbf{W}^*\mathbf{H}^*$. By Lemma B.2, we have

$$\mathbf{W}^{*\top} \mathbf{W}^* = \frac{\lambda_{\mathbf{H}}}{\lambda_{\mathbf{W}}} \mathbf{H}^* \mathbf{H}^{*\top} \implies \mathbf{H}^{*\top} \mathbf{H}^* \mathbf{H}^{*\top} \mathbf{H}^* = \frac{\lambda_{\mathbf{W}}}{\lambda_{\mathbf{H}}} \mathbf{H}^{*\top} \mathbf{W}^{*\top} \mathbf{W}^* \mathbf{H}^* = \frac{\lambda_{\mathbf{W}}}{\lambda_{\mathbf{H}}} \mathbf{V} \mathbf{\Sigma}^2 \mathbf{V}^\top.$$

Now by utilizing Lemma A.4, from the above equation we obtain the following

$$\mathbf{H}^{*\top} \mathbf{H}^* = \sqrt{\frac{\lambda_{\mathbf{W}}}{\lambda_{\mathbf{H}}}} \mathbf{V} \mathbf{\Sigma} \mathbf{V}^\top.$$

This together with the first equation in (17) gives

$$\begin{aligned}
\nabla g(\mathbf{W}^* \mathbf{H}^* + \mathbf{b}^* \mathbf{1}^\top) \mathbf{H}^{*\top} &= -\lambda_{\mathbf{W}} \mathbf{W}^* \implies \nabla g(\mathbf{W}^* \mathbf{H}^* + \mathbf{b}^* \mathbf{1}^\top) \mathbf{H}^{*\top} \mathbf{H}^* = -\lambda_{\mathbf{W}} \mathbf{W}^* \mathbf{H}^* \\
&\implies \nabla g(\mathbf{W}^* \mathbf{H}^* + \mathbf{b}^* \mathbf{1}^\top) \sqrt{\frac{\lambda_{\mathbf{W}}}{\lambda_{\mathbf{H}}}} \mathbf{V} \Sigma \mathbf{V}^\top = -\lambda_{\mathbf{W}} \mathbf{U} \Sigma \mathbf{V}^\top \\
&\implies \nabla g(\mathbf{Z}^* + \mathbf{b}^* \mathbf{1}^\top) \mathbf{V} = -\sqrt{\lambda_{\mathbf{W}} \lambda_{\mathbf{H}}} \mathbf{U}.
\end{aligned}$$

Similarly, we can also get

$$\nabla g(\mathbf{Z}^* + \mathbf{b}^* \mathbf{1}^\top)^\top \mathbf{U} = -\sqrt{\lambda_{\mathbf{W}} \lambda_{\mathbf{H}}} \mathbf{V}.$$

Thus, together with (43), $(\mathbf{Z}^*, \mathbf{b}^*)$ with $\mathbf{Z}^* = \mathbf{W}^* \mathbf{H}^*$ satisfies the optimality condition (41), and hence is a global minimizer of $\tilde{f}(\mathbf{Z}^*, \mathbf{b}^*)$ in (37).

Finally, we complete the proof by invoking Lemma C.2. By Lemma C.2 with $\mathbf{Z}^* = \mathbf{W}^* \mathbf{H}^*$, we know that $f(\mathbf{W}^*, \mathbf{H}^*, \mathbf{b}^*) = \tilde{f}(\mathbf{Z}^*, \mathbf{b}^*) \leq f(\mathbf{W}, \mathbf{H}, \mathbf{b})$ for all $\mathbf{W} \in \mathbb{R}^{K \times d}$, $\mathbf{H} \in \mathbb{R}^{d \times N}$, $\mathbf{b} \in \mathbb{R}^K$. Therefore, we must have $(\mathbf{W}^*, \mathbf{H}^*, \mathbf{b}^*)$ to be the global solution of $f(\mathbf{W}, \mathbf{H}, \mathbf{b})$ in (14). ■